A standardized gnotobiotic mouse model harboring a minimal 15-member mouse gut microbiota recapitulates SOPF/SPF phenotypes

Marion Darnaud[1]*, Filipe De Vadder[2], Pascaline Bogeat[1], Lilia Boucinha[1], Anne-Laure Bulteau[2], Andrei Bunescu[1], Céline Couturier[1], Ana Delgado[1], Hélène Dugua[1], Céline Elie[1], Alban Mathieu[1], Tereza Novotná[3], Djomangan Adama Ouattara[1], Séverine Planel[1], Adrien Saliou[1], Dagmar Šrůtková[3], Jennifer Yansouni[1], Bärbel Stecher[4,5], Martin Schwarzer[3§], François Leulier[1,2§], Andrea Tamellini[1*§]

[1] BIOASTER, Institut de Recherche Technologique, 40 avenue Tony Garnier, 69007 Lyon, France

[2] Institut de Génomique Fonctionnelle de Lyon, Université de Lyon, Ecole Normale Supérieure de Lyon, Centre National de la Recherche Scientifique, Université Claude Bernard Lyon 1, Unité Mixte de Recherche 5242, 46 Allée d'Italie, 69364 Lyon, Cedex 07, France

[3] Laboratory of Gnotobiology, Institute of Microbiology of the Czech Academy of Sciences, 54922 Nový Hrádek, Czech Republic.

[4] Max von Pettenkofer Institute of Hygiene and Medical Microbiology, Ludwig-Maximilians-University of Munich, 80336 Munich, Germany.

[5] German Center for Infection Research (DZIF); Partner Site Munich.

[§]Co-Senior authorship

*Corresponding author: gnotobiology@bioaster.org

Keywords: Gnotobiology; minimal mouse gut microbiota; standardization; bacterial isolation; phenotype.

Abstract

Mus musculus is the classic mammalian model for biomedical research. Despite global efforts to standardize breeding and experimental procedures, the undefined composition and interindividual diversity of the microbiota of laboratory mice remains a limitation. In an attempt to standardize the gut microbiome in preclinical mouse studies, we developed a simplified mouse microbiota composed of 15 strains from 7 of the 20 most prevalent bacterial families representative of the fecal microbiota of C57BL/6J Specific (and Opportunistic) Pathogen-Free (SPF/SOPF) animals and derived a new standardized gnotobiotic mouse model called GM15. GM15 recapitulates extensively the functionalities found in the C57BL/6J SOPF microbiota metagenome, and GM15 animals are phenotypically similar to SOPF or SPF animals in two different facilities. They are also less sensitive to the deleterious effects of post-weaning malnutrition. The GM15 model provides increased reproducibility and robustness of preclinical studies by limiting the confounding effect of fluctuation in microbiota composition, and offers new opportunities for research focused on how the microbiota shapes host physiology in health and disease.

Introduction

The intestinal microbiota is a complex and dynamic community largely composed of bacteria whose activity profoundly influences our health and diseases [1]. Advances in sequencing and analytical technologies coupled with improved computing tools have revolutionized the field of host-microbiota interaction [2]. These developments have provided an increased depth and accuracy in the study of intestinal microbial assemblages and activity for correlative studies with human health or disease traits. Despite these sophisticated descriptions of host-microbiome interaction phenomena, the underlying causal mechanisms remain largely elusive [3].

The use of model organisms plays a decisive role in the challenge to move from correlation to causal links in the host-microbiome field as they have long enabled researchers to identify the shared biological functions among living organisms, and facilitated the discovery of conserved molecular mechanisms governing the fundamental principles of biology [4]. Thanks to its genetic and physiological similarities to humans, in addition to its rapid and prolific breeding, the mouse has been a classic mammalian model of choice for the past decades for biomedical research and the host-microbiome field is no exception [5]. While the use of defined genetic backgrounds, as well as the absence of specific pathogens is now a common practice in mouse studies [6], an important confounding factor is the variability in the composition of the intestinal microbiota which can cause marked phenotypical variations among experimental animals and animal facilities [7,8, 9]. This parameter is under the influence of multiple elements such as genetics, diets, biological rhythms and breeding conditions [10]. As a consequence, to restrain microbial diversity, efforts have been made to tailor protocols for microbiota-related mouse studies and to standardize mouse microbiota composition [10, 11, 12, 13, 14].

The mouse gut microbiota richness is usually estimated at more than 300 bacterial genera [5] and common inhabitants of the mouse intestine belong to seven bacterial phyla with *Firmicutes*, *Bacteroidetes* and *Proteobacteria* being the most abundant ones [13, 15, 16]. The first attempt in standardizing the mouse microbial environment (initially to study immunocompromised mouse models) arose in the sixties with the wide implementation of the Specific Pathogen-Free (SPF) hygienic status of mouse husbandries [17]. Nowadays SPF animals are obtained by re-deriving mouse strains by two-cell-stage embryo transfer to SPF recipients and subsequent post-natal inoculation with a cocktail of bacteria devoid of pathogens to homogenize microbial colonization within a given animal facility. SPF, and then SOPF inbred lines (lacking Specific Opportunist Pathogens such as *Staphylococcus aureus* or *Pseudomonas aeruginosa*) now represents the common health standard for experimental mouse breeding [6]. However, despite the global efforts in standardizing the SPF procedures, the undefined nature and important interindividual diversity of the SPF microbiota remains a limitation in host-microbiome studies, since the scientific community still lacks a common SPF

standard cocktail and rather use a facility-specific cocktail of bacteria [10]. Indeed, the microbiota fluctuates a lot with diet and environment, so it is impossible to have the exact same microbiota of SPF mice in two different facilities.

Microbial cultivation and gnotobiology offer attractive strategies to standardize the microbiota of mouse models. Germ-Free (GF) animals (i.e. animals devoid of any living micro-organisms) are the originators of gnotobiotic animals (i.e. animals with a controlled microbiota) obtained by colonization with pure culture or cocktails of bacterial strains [18]. Recent efforts have been put into isolating, cultivating and archiving isolated culture of the dominant members of the mouse microbiota [19]. Gnotobiotic animals can be kept in isolators for several generations and offer the possibility of a strict control of their microbial status. Gnotobiotic models offering different degree of microbial complexity have been developed in the past ranging from mono-colonization (monoxenic animals) to high diversity microbiota models such as conventionalized ex-GF animals using a donor microbiota [10, 13, 20]. Two models have emerged for breeding and long-term experimental purpose: the Altered Schaedler Flora (ASF) model and the recent Oligo-Mouse-Microbiota^{12} (Oligo-MM^{12}) model [21, 22]. These models offer an enlarged microbial potential as compared to monoxenic mice, while keeping the model simple and experimentally tractable as compared to conventionalized animals (SPF or SOPF).

The ASF was developed in the late 70s by adding bacterial strains which better represented the microbiota of conventional mice to the initial Schaedler flora, a minimal microbial consortium that protected ex-GF mice from opportunistic pathogen colonization during breeding [23]. The ASF is composed of 8 defined bacterial strains, which are stable over mouse generations. Most immune parameters are normalized in mice colonized with ASF when compared with SPF mice, but the fact that the strains of the ASF model are not publicly available and that they are not all representative of the dominant members of the mouse microbiota remains an important limitation [10, 13, 21]. In addition, ASF mice differ substantially from SPF mice with respect to intestinal microbial biochemical activities and resistance to opportunistic pathogen colonization, probably owing to the limited phylogenic diversity and metabolic capabilities of the ASF consortium [10, 13, 24]. Recently, the Oligo-MM^{12} model was

developed [22]. It is a minimal microbiota gnotobiotic model composed of 12 defined cultivable mouse commensal bacteria from the miBC collection representing members of the major bacterial phyla of the mouse gut [19, 25, 26]. The community is transmissible and stable over consecutive mouse generations and animal facilities [27] and was recently used to reveal that the intestinal microbiota adapts to environmental changes by short-term effects of transcriptional reprogramming and adjustments in sub-strains proportions and long-term genomic positive selection [28]. Functionally, and unlike ASF, Oligo-MM^{12} offers colonization resistance against *Salmonella enterica* serovar Typhimurium when supplemented with facultative anaerobic bacteria including *Escherichia coli* [22].

In an attempt to standardize preclinical studies in the host microbiome field, we have developed a simplified mouse microbiota that is representative of SOPF microbiota at the functional level and derived a standardized gnotobiotic mouse model called GM15, which phenotypically mimics SOPF and SPF mice under standard dietary conditions in two different animal facilities. We demonstrate that, under conditions of chronic physiological stress such as post-weaning malnutrition on a low-protein diet, a dietary condition triggering stunting, GM15 microbiota shows improved capacities compared to an SOPF microbiota to buffer the deleterious effect of a depleted diet on mouse juvenile growth.

Results

In silico identification of the main bacterial families of a C57BL/6J SOPF fecal microbiota

To define a minimal microbiota containing representative and prevalent bacteria from the gut of C57BL/6J SOPF mice, we analyzed the composition of fecal pellets from 4 C57BL/6J SOPF mice (obtained from Charles River Laboratories, France) by whole-genome sequencing (two females and two males, which were littermates but housed in different cages from weaning at 3 weeks old, and feces were collected at 2 months old in our facility). An average of 13.4 million of paired-end reads was obtained per sample with a length of 300 bp. The metagenomics data sets generated were classified using the Centrifuge software [29] and compared to the RefSeq complete genome database [30], and 20 dominant families consistently present in all mice

were identified (Fig. 1a). The profiling of metagenomic sequencing data pointed out a comparable distribution of bacterial families among the four tested C57BL/6J SOPF mice (Additional file 1: Fig. S1a-b). Moreover, bacterial species identification was possible for genome sequences with good phylogenetic resolution and already referenced in taxonomy databases. Interestingly, among the identified species, *Bacteroides acidifaciens, Clostridium cocleatum, Lactobacillus johnsonii, Ligilactobacillus murinus* and *Limosilactobacillus reuteri* were previously identified as mouse-enriched and dominant intestinal bacteria [19], *Ligilactobacillus murinus*, *Parabacteroides goldsteinii, Clostridium* strains are part of the ASF model [21], and strains of *Enterocloster clostridioformis*, *Limosilactobacillus reuteri* and *Bacteroides caecimuris* are part of the Oligo-MM^{12} model [22].

Isolation and taxonomic characterization of the GM15 bacterial strains

We established four different strategies in order to isolate and culture a maximal number of representative strains of the 20 dominant bacterial families identified by our metagenomic sequencing analysis (Fig. 1b). First, we isolated the most prevalent strains from fecal pellets of C57BL/6J SOPF mice using non-selective agar media. Then, we used antibiotic selection to isolate resistant strains. We also used rumen enrichment to isolate strains from caecal content. Finally, we used fecal pellets of ASF mice to isolate additional strains. We obtained a collection of approximately 400 cultivable bacterial isolates. All isolates were pre-screened by MALDI-TOF MS for dereplication prior to the first taxonomic identification by 16S rRNA gene Sanger sequencing. We selected eleven strains covering seven of the most representative and prevalent families of the intestinal microbiota of C57BL/6J SOPF mice and obtained four additional strains from the DSMZ miBC collection [19] to establish the GM15 consortium that covers most of the dominant bacterial families found in C57BL/6J SOPF animals (Fig.1a-b). Actually, at the family level the GM15 consortium putatively covers 63% of the SOPF consortium, which is more than the putative coverage previously available with ASF and Oligo-MM^{12} models covering respectively 58% and 48%. In summary, GM15 is composed of two strains of *Bacteroidaceae*, one strain of *Tannerellaceae*, six strains of *Lachnospiraceae*, three

strains of *Lactobacillaceae*, one strain of *Erysipelotrichaceae*, one strain of *Ruminococcaceae*, and one strain of *Enterobacteriaceae* (Additional file 1: Fig. S1c). We recently reported the draft genomes of the fifteen strains and alignment against the NCBI database [31] allowed the identification of 12 strains at the species level and 3 strains at the family level [32], which are described as novel taxa in this study.

In silico **functional metagenomics analysis of the GM15 strains**

To gain insights into the functionalities encoded in the individual genomes of the GM15 members, the coding sequences of the 15 strains were converted into their respective protein sequences, which were annotated for clustering into KO (KEGG Orthology) groups. By merging the 15 assembled individual genomes, we found that the GM15 metagenome possesses 3890 non-redundant KO groups covering 44% of all protein coding sequences. Besides, all GM15 strains possessed 3 to 64 unique functions, although *E. coli* Mt1B1 exhibited a vast repertoire of unique KO groups (10^3), indicating that *E. coli* Mt1B1 is responsible for the GM15's functional metagenomic profile at 33%, while the 14 other strains contribute all together at 8% and the 59% remaining are associated to non-unique KO groups (Fig. 1c). It is noteworthy that KEGG module analysis is biased towards gene sets, pathways and functional groups of well-characterized bacteria such as *E. coli*, which is by far the most studied bacterial species to date.

Next, we highlighted the *in silico* functionalities of the 15 selected strains associated with known enzymatic activities in the gut [33] (Fig. 1d). Again *E. coli* Mt1B1 is a major contributor, but each functionality is also covered by other strains at equivalent or lower levels. As expected, the enzymatic activities in the gut are correlated with the phylogenetic membership of the strains. For example, lactobacilli, which are a major part of the lactic acid bacteria group, the principal contributor to lactate dehydrogenase [34], clustered together. Additionally, *Lachnospiraceae* clustered with *Ruminococcaeae* and *Erysipelotrichaceae*, which include mainly bacteria with sporulation capabilities [35, 36, 37]. Finally, *Bacteroides* clustered with *Parabacteroides*, whose species are predominant in the colonic mucus barrier

and promote mucinase activity [38], and are significant producers of succinate, a major metabolic by-product [39, 40]. Thus, different strains of a bacteria family and of other closely related bacterial families are capable of the same enzymatic activities in the gut. This can be essential for the generation of simplified non-specific gnotobiotic models.

Then, we determined the functional coverage of the GM15 metagenome (i.e. the sum of the genomes of the 15 strains) relative to the KEGG modules of C57BL/6J SOPF mouse microbiota (covering 47% of all protein encoding sequences) found in our initial metagenomic analysis (Fig.1a). In addition, the KEGG modules from the Oligo-MM^{12} and ASF microbiota (covering respectively 46% and 43% protein coding sequences) were included for comparative analysis, as these consortia were previously used to generate gnotobiotic mice with a stable and defined mouse-derived microbiota [25, 41]. The presence and completeness of KEGG modules was determined for each metagenome and used for hierarchical clustering (Fig. 1e). One cluster contained highly conserved modules in all mouse models (Fig. 1e, cluster 4; Additional file 2: Table S1), including 140 pathways. We also identified clusters of modules that were not represented among the ASF and Oligo-MM^{12} consortia, but specifically common to GM15 and SOPF (Fig. 1e, clusters 9 and 6; Additional file 2: Table S1), comprising a total of 155 pathways indicating that qualitatively the GM15 metagenome covers functionalities found in SOPF microbiota that were lacking in ASF and Oligo-MM^{12} models. Quantitatively, the defined consortia of GM15, Oligo-MM^{12} and ASF covered respectively 72, 54 and 48% of the KEGG modules of the C57BL/6J SOPF microbiome suggesting a superior functional potential of the GM15 community as compared to Oligo-MM^{12} and ASF models. Thus, taken collectively our *in silico* analysis suggests that the GM15 community carries a significant potential for enzymatic activities in the gut and recapitulates widely the functionalities found in C57BL/6J SOPF murine metagenome.

Monitoring and stability assessment of GM15 gut microbiota

To explore *in vivo* the functional potential of the GM15 community, we used our SOPF colony to produce GF mice and next generated GM15 gnotobiotic animals. First, we investigated

whether the GM15 consortium can stably colonize the mouse intestine over several generations. To this end, we developed a strain-specific quantitative polymerase chain reaction (qPCR) microfluidic assay, which allows simultaneous absolute quantification of the 15 strains, along with the global bacterial load in a given biological sample (Additional file 3: Table S2). Fecal samples from GF and SOPF mice were used as negative and positive controls. Only *Enterocloster clostridioformis* YL32, which was obtained from the DSMZ miBC collection, was not detected in our SOPF mice. Co-monitoring of specific and total bacteria aimed to detect any bacterial load imbalance caused by a contamination in gnotobiotic isolators.

Eight-week-old GF mice (five breeding pairs; GM15 founders, F0; Additional file 4: Fig. S2a) were inoculated by oral gavage with a fresh frozen mixture of the 15 strains and bred in sterilized positive pressure isolators up to the F9 filial generation. All strains except *Subtilibacillum caecimuris* MD335, *Longibacillum caecimuris* MD329, and *Irregularicoccus caecimuris* MD308 were above the detection limit of our qPCR microfluidic assay in the fecal samples of most individual mice (GM15 founders and progenies from the 9 consecutive generations; Additional file 5: Fig. S3a; Fig. 2a). *Anaerotruncus colihominis* JM4-15, *Clostridium* ASF 356, *Clostridium* ASF 502, and *Clostridium cocleatum* I50 were occasionally below detection limit but the detection of the remaining strains was reproducible between fecal and caecal samples from individual mice in the second filial generation (Additional file 5: Fig. S3b; Fig. 2a). Taken together, these results indicate a stable colonization and effective vertical transmission of at least 12 strains out of the 15 inoculated. Based on the results of our qPCR assay, we consider that the 3 remaining strains: *Subtilibacillum caecimuris* MD335, *Longibacillum caecimuris* MD329, and *Irregularicoccus caecimuris* MD308, either did not efficiently colonize the animals, live in the caecum or the colon below the detection limit of our qPCR assay, or predominantly live in other gastrointestinal niches than those sampled.

Next, we evaluated the effect of aging on the GM15 community by following individual mice of the first filial generation between 2 and 12 months of age (Additional file 4: Fig. S2a). Overall, no changes in the qualitative and quantitative composition of the GM15 consortium

were detected (Fig. 2b). Then, we asked if the composition of the GM15 community was modulated by substituting the breeding diet by an alternative maintenance diet. This alternative diet is quasi isocaloric but its nutritional composition differs by 1.3 and 1.6-fold fewer proteins and lipids respectively, and 1.2-fold more carbohydrates than the breeding diet. An alternative diet was administrated to 8-week-old GM15 mice for 4 weeks. We collected fecal samples before diet change, after 2 and 4 weeks, and again after 4 weeks back to the breeding diet (Additional file 4: Fig. S2a). We did not detect any significant changes in the GM15 composition under these conditions (Fig. 2c). Additionally, successful fecal microbiota transplantation (FMT) from GM15 founders to GF mice was confirmed by strain-specific qPCR of the ex-GF mice feces collected at week 1, 2 and 3 post-transplantation (Additional file 4: Fig. S2a; Fig. 2d).

When all the data are analyzed together, we notice a limited fluctuation (maximum 2 Log10-fold change) of each member of the GM15 gut microbiota's load among the conditions tested (Fig. 2e). Therefore, we conclude that the GM15 community is stable upon adult colonization, among filial generations, during aging, upon mild dietary fluctuations and can be transmitted efficiently by FMT.

The GM15 microbial community recapitulates SOPF macroscopic phenotype

GF and published gnotobiotic mice display anatomical alterations compared to SOPF mice, such as enlarged caecum, along with physiological and metabolic differences [22, 42]. To phenotypically assess the gnotobiotic GM15 model, we designed a comparative study to evaluate the steady state macroscopic, immune, metabolic and endocrine phenotypes of GF, SOPF and GM15 mice. In addition, all phenotyping was achieved across two generations, F1 and F2, to strengthen data analysis.

Initially, we evaluated the reproduction performance of the GM15 model by recording the period from mating to offspring delivery (Fig. 3a), the number of pups per litter (Fig. 3b), and the perinatal mortality (Fig. 3c). GM15 mice behaved like SOPF mice with the exception of one less progeny per mean litter. Indeed, the distribution of progeny per litter in GM15 mice

ranged more evenly from 3 to 9 pups compared to SOPF mice, whose mean number of pups per litter was mostly centered on 7 or 8 pups. Then, we quantified the food intake relative to body weight after weaning at 4 weeks of age and observed no significant difference between the three groups despite a marked increased variation among GF animals which is not detected in GM15 and SOPF animals (Fig. 3d). Next, we studied post-natal growth parameters. Male and female GM15 animals gained weight (Fig. 3e) and size (Fig. 3f) like SOPF mice, although the growth curves from the two sexes differ. We then studied internal organ size. As expected, the characteristic caecum enlargement seen in GF animals was reduced in GM15 mice (Fig. 3g). The weights of GM15 and SOPF brain, liver and spleen were equivalent and larger than those of GF mice (Fig. 3g). Bone size was also identical in GM15 and SOPF mice and larger than that of GF mice (Fig. 3h). Taken together, these results confirm that the gut microbiota contributes to somatic tissue growth [43, 44], and that the GM15 simplified microbiota is sufficient to largely recapitulate the breeding and growth performance of SOPF mice by compensating the physiological limitations of GF mice.

The GM15 simplified microbiota partially restores SOPF immune phenotype

It is now well established that host-specific bacteria consortia influence intestinal and systemic immune maturation [45, 46]. We thus profiled the basal immune parameters of GM15 animals and compared them to SOPF and GF animals at 7-8 weeks of age. For that purpose, we analyzed immunoglobulins levels in feces and sera and cytokines levels in serum. In parallel, we assessed viable leukocytes by measuring CD45+ cell count and analyzed T cells, B cells, NK cells and monocytes or dendritic cells (DC) populations frequencies in whole blood and several lymphoid organs (spleen, thymus, Peyer's patches (PP) and mesenteric lymph nodes (MLN)).

In our study, no difference was observed between the 3 groups of mice for serum IgG1 levels and all IgG2a levels were below levels of detection. Of note, IL-1b, IL-10, IL-12p70, and IL-17f, which are cytokines involved in autoimmune and inflammatory bowel diseases were not

impacted. In addition, DC in MLN, CD4+ and CD8+ T cells in whole blood and spleen, and B cells in spleen did not show any modulations between the 3 groups either (data not shown).

Among already described immunodeficiencies in GF mice [47, 48], we observed that the GM15 community restored the production of IgA in the gut and in serum, and IgG2b in serum, at levels equivalent to those detected in SOPF mice (Fig. 4a-c). Notably, the highest levels of circulating IgA were not correlated with the highest levels of fecal IgA, and intragroup variability was not related to gut microbiota composition, which was homogeneous between individuals. In addition, circulating IL-22 levels, which is one of the key intestinal cytokines, were restored as well in GM15 mice (Fig. 4d). Furthermore, it has been previously shown that isolated lymphoid structures such as PP and associated cellularity were strongly increased with microbiota diversity whereas the total cell numbers in MLN were comparable between GF and SPF mice [49, 50]. As described in literature, the number of PP collected where higher in SOPF mice compared to GF and partially restored in GM15 mice (Fig. 4e). No or minor difference were observed between the 3 groups for CD45+ cell count (Fig. 4f). A slight increase was observed in CD45+ cell count in SOPF compared to GF mice with apparent intermediate CD45+ cell count in GM15 mice in spleen, thymus and PP and with no difference in MLN (Fig. 4g-i). In 2018, Kennedy *et al.* published an overview of the literature describing the main immune cell populations modifications observed in GF mice in different organs [51]. Interestingly, the great majority of populations impacted showed similar frequencies in GM15 mice and SOPF compared to GF mice (Additional file 6: Fig. S4a-e). Monocytes in whole blood, CD4+ T cells in thymus, CD8+ T cells in MLN, DC in PP, B cells in MLN and whole blood and NK cells in spleen were restored in GM15 mice. Among those cell populations, only B cells in GF whole blood showed higher concentrations compared to those described in the literature [46]. Our observations of NK cells decrease in spleen and DC increase in PP in GF mice compared to SOPF mice were not yet described.

Minor differences were observed between GM15 mice and SOPF but not with GF mice for DC in spleen and CD4+ T cells in PP, whereas both populations were described to be decreased in GF mice (Additional file 6: Fig. S4b, e). Only NK cells in PP showed similar and

increased frequencies in GM15 and GF mice compared to SOPF mice (Additional file 6: Fig. S4e). In a same way, minor differences were observed as well for some serum immunoglobulins level. In our model, IgG3 levels were increased in GM15 mice compared to GF and SOPF mice and IgM levels were slightly increased in GM15 mice compared to SOPF (Fig. 4j-k). Of note, those immunoglobulins levels were lower in our SOPF mice than levels already described in SPF mice [47, 48].

Surprisingly, a first set of GM15 mice (F1 and F2) born to a colonized mother presented elevated levels of IgE in serum compared to GF and SOPF mice (Fig. 4l). Such IgE levels may result from parasitic infections, immunodeficiencies or long-lived IgE producing plasma cells generated by food antigens in mice with low-diversity microbiota during early life [47, 52, 53]. Of note, unlike previous study our GF mice did not show increased IgE levels compared to SOPF [47]. Independent tests following FELASA guidelines (CR EU RADS, France) rejected the infection hypothesis of the GM15 mice, which were negative for ectoparasites and endoparasites, respiratory and intestinal specific pathogenic bacteria and infectious agents, as well as viruses. To confirm this observation, we sampled again serum from additional GM15 animals (F5 and F6) several months after the initial test and quantified the IgE circulating levels with two independent methods. Although both Luminex and ELISA assays were calibrated against purified mouse IgEκ, they provided very different ranges of IgE values. However, both methods indicate that this second set of GM15 animals had normal levels of circulating IgE (Fig. 4m; Additional file 6; Fig. S4f). We also found that circulating IL-17a levels were increased in the first set of GM15 mice compared to SOPF and GF mice (Fig. 4n), but the IL-17a levels were much lower in the second set of GM15 animals and ultimately similar to SOPF mice, apart from one outlier (Fig. 4o).

Taken collectively, our results indicate that the GM15 community is sufficient to restore some key parameters of the immune response lacking in GF animals such as modified levels of serum and fecal IgA, serum IgG2b, serum IL-22, PP number, CD45+ cell count and immune cell populations frequencies in different organs close to that detected in SOPF animals.

Low-complexity GM15 microbiota shares more metabolic traits with SOPF than GF mice

The gut microbiota influences multiple host metabolic pathways by providing metabolites to its host and also shapes inter-organ communication within the body by influencing the production and activity of endocrine signals [54, 55]. One-dimensional proton nuclear magnetic resonance spectrometry (^{1}H NMR) was previously applied to investigate how the gut microbiota impacts host metabolism using mouse models [56, 57], or human cohorts [58]. Using this technology, we analyzed the metabolic profile of plasma samples from GF, GM15 and SOPF mice and were able to quantify a total of 57 polar metabolites and 5 non-polar metabolites. It could be seen that only few of them were significantly affected by sex (Additional file 7: Table S3). A principal component analysis based on quantified polar metabolites showed sequential alignment on first principal component (9.2% of total variance) according to microbiota complexity of GF, GM15 and SOPF samples, independently of F1 and F2 generations (Fig. 5a). The metabolite composition of GF plasma resulted only from the host metabolic activity and represented a basal phenotype. Conversely, the SOPF mice harboring a very diverse gut microbiota, exhibited a larger panel of metabolic activities based on host-bacterial and bacterial-bacterial interactions. In-between, the GM15 low-complexity community contributed in a lower extent to the metabolic phenotype. We performed the equivalent statistical analysis using binned NMR spectra instead of quantified metabolites and as expected we obtained the same results (Additional file 8: Fig. S5). Next, we performed a discriminant analysis across all samples to highlight the specific metabolic signatures of each group. Nine metabolites emphasized significant variation, although it is noteworthy that the calculated distance placed GM15 closer to SOPF than to GF (Fig. 5b). Dimethylamine and isopropanol tended toward GF mice, but concentrations were low and taken alone there was no difference between groups (Additional file 7: Table S3). As previously reported, GF mice had higher plasma levels of glycine [59] and reduced plasma acetate concentration [60]. On the contrary, SOPF mice harboring a diverse microbiota had higher plasma levels of acetate, dimethyl sulfone, 3-hydroxybutyrate and propionate [54, 61]. As for GM15 mice, less methanol and more citrate were detected. Interestingly, methanol may occur as a result of fermentation by gut bacteria

and can stimulate citric acid fermentation [62, 63]. Thus, the simplified gut microbiota of GM15 mice may produce less methanol and/or microbially-produced methanol may be used to form citrate. These specific metabolic signatures may be used in the future as a panel of biomarkers to identify the GM15 model. Besides, the analysis of the plasma non-polar metabolites indicated that GM15 colonization was sufficient to reduce free cholesterol and phosphatidylcholine as observed in SOPF mice (Fig. 5c). The three additional non-polar metabolites detected were equivalent in all mice (Additional file 7: Table S3).

Finally, we investigated the circulating levels of key metabolic hormones and growth factors. To allow different types of analyses using the same blood sample, mice were not fasted. Ghrelin was below limit of detection for all groups, and glucagon, insulin and leptin did not show any difference between GM15 and GF mice, whereas levels detected in SOPF mice were similar to those previously published under basal conditions [64, 65, 66] (data not shown). However, as compared to levels detected in GF animals the GM15 gut microbiota was able to restore the levels of circulating insulin growth factor 1 (IGF-1) to the levels observed in SOPF animals. IGF-1 is an essential growth factor promoting systemic and tissue growth [67, 68] and this observation correlates well with the improved macroscopic growth of GM15 mice compared to GF animals (Fig. 5d, Fig. 3e-h). Corticosterone levels, which are high in GF and low in SOPF animals were also normalized by GM15 bacterial colonization [69] (Fig. 5e), indicating that GM15 community seems as efficient as a complex SOPF microbiota at utilizing host metabolites and promoting steroidogenesis and growth factor production.

Collectively, our results reveal that GM15 animals stand out from GF mice and recapitulate many of the SOPF metabolic features even though some differences exist.

GM15 mice are less sensitive to diet-induced stunting than SOPF mice

Previous work by our lab and others [70, 71, 43] has shown that the gut microbiota influences pathogenesis associated to chronic undernutrition, particularly diet-induced stunting. Consequently, we sought to study our newly-established gnotobiotic mouse model under a severe nutritional stress, induced by a nutrient-depleted diet (containing 4% protein and 2%

lipids) expected to trigger stunting. We thus fed male mice a breeding diet (BD) or a depleted diet (DD) from post-natal day 21 (i.e. the day of weaning) until post-natal day 56.

As shown in Fig. 6a-b and similarly to our previous observation (Fig. 3e-f) GM15 and SOPF mice grew well on the BD as they show similar body weight and size gains. Next, we confirmed that the DD triggered an almost full stunting of both the juvenile GM15 and SOPF mice, characterized by the flattening of their weight and size curves (Fig. 6a-b). However, the GM15 mice performed better in terms of growth as both their body weight and size were significantly less impacted than SOPF animals by the DD. While the caecum of GM15 was enlarged (Fig. 6c, Additional file 9: Fig. S6a), this variation could not account for the total weight difference between GM15 and SOPF animals. We thus compared the sizes and weights of nine other organs (Fig. 6d-f, Additional file 9: Fig. S6b-g) in order to account for these variations and using two-way ANOVA, we confirmed that diet was the main driver of the growth phenotype. However, we found that the increase in body size observed in GM15 mice on the DD could be correlated to a significant increase in the size of the tibia (Fig. 6d). Although we did not find any other significant differences in other single organ size or weight between GM15 and SOPF animals on DD, we observed a clear tendency of an increase in GM15 compared to SOPF animals for most parameters tested (Fig. 6e-f, Additional file 9: Fig. S6b-g). We tested this tendency by integrating all the phenotypical parameters in a Principal Component Analysis (PCA). We first established which parameters were correlated to the phenotype (Additional file 9: Fig. S6h), thus excluding brown adipose tissue from the analysis as a non-correlating parameter. The PCA revealed that, under BD, the GM15 phenotype was part of the spectrum of the SOPF phenotype (Fig. 6g). However, under DD, there is a clear shift between the GM15 and SOPF phenotypical space (Fig 6g, dotted lines). Our results thus indicate that under nutritional stress, GM15 microbiota buffers diet-induced stunting slightly more effectively than a SOPF microbiota. As IGF-1 is an important driver of the diet and microbiota-mediated growth promotion [43], we assessed IGF-1 levels in animals and while the levels massively drop in the DD conditions, we did not detect any difference between GM15 and SOPF mice at day 56 on the DD (Fig. 6h). However, we cannot exclude that slight variation in size between GM15

and SOPF animals on DD results from a differential secretion of IGF-1 before day 56, when the growth rate of the animal is maximal (Fig. 6a-b).

Taken together, our data show that animals bearing the simplified GM15 microbial community perform similarly when compared to animals bearing a complex SOPF microbiota under non stressful conditions. However, the GM15 microbiota seem partially protective against the deleterious effects of chronic undernutrition, as compared to SOPF mice.

The GM15 model growth and diet-induced stunting phenotypes are reproducible in another gnotobiotic facility

Reproducibility is an imperative to preclinical research especially in the microbiome field. Therefore, to test the transferability and reproducibility of the GM15 model, we established it in a second gnotobiotic facility (Facility 2 - Laboratory of Gnotobiology at Institute of Microbiology of the Czech Academy of Sciences, Novy Hradek, Czech Republic). We colonized GF animals with the GM15 consortia using the same protocol described for facility 1. Using qPCR microfluidic assays, we analyzed the bacterial titers in fecal samples of the newly generated GM15 animals and control SPF animals from the same facility, bred in the same condition as GM15 animals (Additional file 4: Fig. S2b). Similarly to GM15 colonized mice at Facility 1, all strains except *Subtilibacillum caecimuris* MD335, *Longibacillum caecimuris* MD329, and *Irregularicoccus caecimuris* MD308 were above the detection limit in GM15 individual mice (Fig 7a). GM15 strain levels in facility 1 and 2 were very similar (Fig. 7b) demonstrating that the GM15 model can be effectively transferred and established in a reproducible manner in different gnotobiotic facilities.

We next compared the titers of each strain individually in GM15 and SOPF/SPF animals from both facilities. Besides *Clostridium* sp. MD294 and *Clostridum* sp. MD300, which are less well colonizing GM15 animals than SPF/SOPF animals in both facilities, there was a clear general tendency of more similar fecal titers in GM15 animals as compared to their titers in SPF/SOPF animals between facilities (Fig. 7b and Additional file 10: Fig. S7a) suggestive of more reproducible microbiota in GM15 animals. As a control gnotobiotic mouse model with a

significantly different microbiota from GM15 (Fig. 1e), we generated Oligo-MM^{12} animals in facility 2. As previously reported [27], Oligo-MM^{12} gnotobiotic animals were successfully established in facility 2 and the *Bifidobacterium animalis* YL2 and *Acutalibacter muris* KB18 strains were again not detected (Additional file 10: Fig. S7b).

Then, we conducted a comparative study to evaluate the growth phenotypes of SPF, Oligo-MM^{12} and GM15 mice in facility 2 on standard breeding diet. Both GM15 and Oligo-MM^{12} female mice grew well compared to SPF females with female Oligo-MM^{12} to gain weight slightly faster than GM15 females (Fig. 8a). GM15 and Oligo-MM^{12} males also grew slightly better than SPF males (Fig. 8e). Importantly, GM15 growth phenotypes (mean daily body weight and size gains) were more reproducible between facility 1 & 2 than for SOPF/SPF animals which significantly differed between the facilities (Fig. 8b, f).

These macroscopic observations correlated well with internal organ size: the weights of GM15 and Oligo-MM^{12} animals' brain, kidneys, liver, spleen, muscles, and adipose tissues were equivalent in females (Additional file 11: Fig. S8a) or larger in males (Additional file 11: Fig. S8b) than those of SPF mice. Of note, female Oligo-MM^{12} mice had less WAT and more BAT than GM15 and SPF females and, as expected, both gnotobiotic models had a slight cecum enlargement compared to SPF animals yet their cecum size was significantly reduced as compared to the one of GF animals (Additional file 11: Fig. S8a; and see Fig. 3g for GF). Finally, bone size was increased in both gnotobiotic models of both sexes compared to SPF animals with a more pronounced and statistically robust effect in GM15 mice (Fig. 8c, g).

Taken together these results establish that the macroscopic phenotypes of GM15 mice identified in facility 2 are similar to those from facility 1. Importantly, when comparing the results from the two facilities we could also establish that GM15 mice growth phenotypes are more reproducible between facilities than SOPF/SPF animals. Our results also confirm that gnotobiotic models carrying a minimal microbiota compensate effectively the physiological limitations of GF mice and mimic (when not improving) the macroscopic growth phenotypes of SOPF/SPF animals. Such results correlate well with the endocrine markers of growth IGF-1 and IGFBP3 (Fig. 8h) and are not due to a difference in relative food intake between conditions

(Additional file 11: Fig. S8c). Finally, our results also suggest that each gnotobiotic model carries its own phenotypical characteristics at steady state: a specific lower WAT-higher BAT phenotype in Oligo-MM^{12} females and an increased bone growth in GM15 animals.

In facility 1, we reported that GM15 microbiota is partially protective against the deleterious effects of chronic undernutrition, as compared to SOPF mice (Fig. 6). To test the reproducibility of this phenotype in another facility, we submitted GM15 males from facility 2 to the same severe nutritional stress, by using the same nutrient-depleted diet as in facility 1 shown to trigger severe stunting after weaning (Fig. 6). This time, we also tested Oligo-MM^{12} males under the same dietary regime. As in facility 1, all animals developed a macroscopic stunting phenotype and a related bone and endocrine markers alterations (Fig. 8e-h). Interestingly, as in facility 1, and despite a marked stunting phenotype, we detected an improved body weight and body size gain of GM15 males on the depleted diet compared to SPF males (Fig. 8e, f). This observation is confirmed by an increased size of bones (Fig. 8g) and IGF-1 and IGFBP3 levels in sera (Fig. 8h) in GM15 males as compared to SPF animals. Of note, on the depleted diet, Oligo-MM^{12} males also performed significantly better than SPF animals, a very similar phenotype to GM15 males, suggesting that this buffering effect is not a unique attribute of the GM15 model.

The GM15 model immune and metabolic phenotypes are reproducible in another gnotobiotic facility

To follow up on our initial phenotyping of animals from facility 1, we studied specific immune and metabolic parameters of SPF, Oligo-MM^{12} and GM15 animals from facility 2. As previously reported in facility 1, the GM15 community supports IgA (both serum and fecal levels), IgG2b, IgG3 and IgE production (Additional file 12: Fig. S9a). Of note, we confirmed in facility 2 the similar IgE levels between GM15 and SPF animals using both Luminex and ELISA methods (Additional file 12: Fig. S9a and b). GM15 also supports increased levels of IgM and IgG2a, and supports circulating levels of IL-22 and IL-17a as in SPF animals (Additional file 12: Fig. S9a, c). Collectively, these results confirm, in another facility, that the GM15 community is

sufficient to restore key parameters of immune system development and maturation known to be altered in GF animals. Finally, while comparing GM15 and Oligo-MM^{12} models, the GM15 consortium seemed more prone to support immunoglobulin (fecal and serum IgA, serum IgG2b, IgE, IgG2a, IgG3 and IgM) and interleukine (IL-17a and IL-22) production. Interestingly, these features are regulated upon recognition of intestinal microbiota (45, 47, 48, 72). Finally, a particularity of the Oligo-MM^{12} model was its lower circulating levels of IgE, IgG2a, serum IgA and IL-22 compared to SPF and GM15 mice, illustrating a difference in the immune phenotype of the two gnotobiotic models.

To explore the metabolic profiles of GM15, SPF and Oligo-MM^{12} animals in facility 2, we conducted ^{1}H NMR on plasma samples as previously performed on plasma of facility 1 animals. We were able to quantify a total of 54 polar metabolites and 5 non-polar metabolites (Additional file 7: Table S3). Principal component analysis based on quantified polar metabolites showed a sequential alignment according to sample type (GM15, SPF or Oligo-MM^{12}) on the first and second principal components (9.6% and 7.1% of total variance respectively, and 6.3% on the third component; Additional file 12: Fig. S9d) and calculated distance placed SPF sample quasi-equidistant to GM15 and Oligo-MM^{12} samples, with each gnotobiotic model showing a distinct metabolic phenotype strongly resembling that of SPF animals. Polar metabolites were more prone to sex and group effects in facility 2 than in facility 1, but lipids were stable and male to female difference (fold change > 1.3 and p-value < 0.05) was only seen in triacylglyceride in SPF mice from facility 2 (and in GF mice from facility 1). Like in facility 1, GM15 and SPF mice shared many similarities and a lower methanol/citrate ratio was again observed in GM15 mice. Metabolites profiles of GM15 and Oligo-MM^{12} mice were also similar, non-polar metabolites were equivalent in all mice except triacylglyceride which was higher in SFP mice. Finally, we noticed as many differences between GM15 animals as between SOPF and SPF mice across the two facilities. Such variability might be due to the different breeding diets used in the two facilities, and the fact that mice were housed in isolators in facility 1 rather than in individual ventilated cages in facility 2.

Taken collectively, these results obtained in a second gnotobiotic facility confirm that gnotobiotic models carrying minimal microbial consortia such as the GM15 community mimic SPF/SOPF animal phenotypes at steady states.

Discussion

Here we describe GM15, a simplified and controlled murine gut microbiota and its related C57BL/6J gnotobiotic mouse model. The GM15 community is composed of pure cultures of 15 strains from 7 of the 20 most prevalent bacterial families present in the fecal microbiota of C57BL/6J SOPF mice. GM15 carries significant potential for enzymatic activities in the gut and recapitulates extensively the functionalities found in C57BL/6J SOPF gut microbiome. *In vivo*, GM15 is stable upon adult colonization for up to 12 months, during natural transmission among 9 filial generations, upon mild dietary fluctuations, can be transmitted efficiently by FMT and can be re-established efficiently in another gnotobiotic facility. GM15 compensates breeding, growth, immune, endocrine and metabolic limitations of GF mice and recapitulates many SOPF animals´ phenotypical features in a reproducible manner in two gnotobiotic facilities.

As all experimental models, GM15 has its limitations and microbiota standardization, which is essential for establishing robust causal relationships between a microbiota configuration and a host trait, may decrease the translational potential of the observation. Despite being macroscopically similar, GM15 and SOPF animals differ in specific immune and metabolic signatures. This is not particularly surprising given the marked reduced microbial diversity that the GM15 model carries compared to SOPF microbiota (15 strains versus hundreds of species in SOPF animals). The specific immune and metabolic signatures of the GM15 model pave the way to further studies aiming at defining if the presence or absence of specific community members triggers these phenotypes. Besides, the GM15 model offers new insight for gnotobiotic research as a complementary model to other murine bacteria-based models like ASF and Oligo-MM[12]. Indeed, GM15 covers more functionalities of the C57BL/6J

SOPF microbiome as compared to the other two models. For instance, microbiota-mediated resistance to *Salmonella enterica* serovar Typhimurium infection may be tested in GM15 animals and compared to ASF and Oligo-MM^{12} animals as recently done by Stecher and colleagues [22]. Yet, our phenotypical comparison between the GM15 and Oligo-MM^{12} models reveal that both gnotobiotic animals largely mimic SPF/SOPF animal phenotypes at steady state and both show an improved response to chronic undernutrition and as a result a milder diet-induced stunting phenotype. Each model also carries its intrinsic phenotypical features: improved bone growth and immune maturation in GM15 animals and improved weight gain dynamics upon juvenile growth and a lower WAT/higher BAT ratio seems a hallmark of the Oligo-MM^{12} model. These phenotypical differences also translate into the metabolic phenotype of these animals, which seem more distant between them, yet still close to the SPF/SOPF metabophenotye but in their respective manner. These observations therefore pave the way to study the underlying symbiotic mechanisms which support these shared and/or unique phenotypes. These controlled minimal microbiota models are unique tools to study these mechanisms in mice with an unprecedented microbial resolution.

Taken together our results establish that GM15 is a new controlled preclinical model phenotypically similar to SOPF with the potential to ensure an increased reproducibility and robustness of preclinical studies by limiting the confounding effect of microbiota composition fluctuation and evolution. Importantly, the reduced microbial complexity of the GM15 community, the efficacy of its transfer to GF animals in different facilities, the tractability of its members and the control offered to the scientist on its composition over time allow easy quantification and recording of short and/or long-term gut microbiota dynamics, a current limit when using SPF/SOPF animals. Importantly, it was recently exemplified that minimal microbial communities do naturally evolve in gnotobiotic animals bred on chow diet or upon dietary challenges [28]. In order to ensure optimal reproducibility of preclinical works, it is advisable to regularly re-establish the models using fresh frozen bacterial samples and new GF animals to avoid drift and/or selection of variants in the microbial community. The GM15 model, by its low complexity, also offers the possibility to use it as a template for establishing further complex

consortia, e.g. by complementing it with representative strains of the missing prevalent bacteria family found in SOPF microbiota such as *Deferribacteraceae*, *Oscillospiraceae*, *Clostridiaceae* and *Eubacteriaceae*. Indeed, upon manipulation of the GM15 community composition, the correlation of such dynamics with fluctuating host traits allows the establishment of causal relationships between specific microbiota members and host traits. GM15 model offers exciting perspectives for improvement. Actually, under stressful nutritional environment, the simplified GM15 microbiota performs slightly better than a complex SOPF community in terms of physiological host response. We have previously identified a lactobacilli strain that is capable of buffering the deleterious effects of such challenge in monocolonized mice [43]. Interestingly, out of its 15 strains, GM15 microbiota contains 3 lactobacilli strains. Further genetic manipulations coupled to gnotobiotic studies focusing on modifying the lactobacilli components of GM15 may pave the way to understanding how this minimal bacterial community buffers the host response to chronic undernutrition.

In conclusion, our study establishes that the GM15 model offers new possibilities for preclinical research focusing on host-microbes and microbe-microbe interactions, and how the microbiota shapes the environmental impact on health and diseases or drug efficacy.

Methods

Bacterial strains isolation and identification

Fresh caecal contents and fecal pellets of C57BL/6J SOPF mice (Charles River Lab., France) were resuspended (1/10 wt/vol) in reduced broth media for direct dilution plating on agar plates and growth at 37°C under anaerobic atmosphere (90% N_2, 5% H_2, 5% CO_2). *Lactobacillus johnsonii* MD006 was isolated on MRS agar. *Ligilactobacillus murinus* MD040 and *Parabacteroides goldsteinii* MD072 were isolated on Colombia CNA agar with 5% sheep blood. *Bacteroides acidifaciens* MD185 and *Irregularicoccus caecimuris* MD308 were isolated on GAM agar. *Bacteroides caecimuris* MD237 and *Limosilactobacillus reuteri* MD207 were isolated on GAM agar supplemented respectively with 32 µg/mL vancomycin and 32 µg/mL

erythromycin. *Subtilibacillum caecimuris* MD335 and *Longibacillum caecimuris* MD329 were isolated on M2GSC agar (modified Hobson, containing (per 100 mL) 1 g of casitone, 0.25 g of yeast extract, 0.4 g of NaHCO3, 0.2 g of glucose, 0.2 g of cellobiose, 0.2 g of soluble starch, 30 mL of clarified rumen fluid, 0.1 g of cysteine, 0.045 g of K2HPO4, 0.045 g of KH2PO4, 0.09 g of (NH4)2SO4, 0.09 g of NaCl, 0.009 g of MgSO4.7H2O, 0.009 g of CaCl2, 0.1 mg of resazurin, and 1.5 g agar). *Subtilibacillum caecimuris* MD335, *Longibacillum caecimuris* MD329, and *Irregularicoccus caecimuris* MD308 were isolated from caecal contents, the rest from fecal pellets. Fecal pellets of ASF mice (Taconic, USA) were cryopreserved at -80°C, and then resuspended in reduced broth media for direct FMT in GF mice. Fresh caecal content and fecal pellets were resuspended in reduced broth media for direct dilution plating on agar plates and growth at 37°C under anaerobic atmosphere (90% N_2, 5% H_2, 5% CO_2). *Clostridium* sp. MD294 and *Clostridium* sp. MD300 were isolated on M2GSC agar, respectively from caecal content and fecal pellets of ASF mice. For identification of isolates, colonies were pre-screened for dereplication by MALDI-TOF MS (Vitek MS, Biomérieux) according to the manufacturer's instructions and database enrichment using RUO mode [73]. Then, gDNA was extracted from pure cultures and analyzed by 16S rRNA gene sequencing (GATC Biotech). Following Edgar's recommendation [74], a full-length 16S rRNA sequence similarity ≥99% using either NCBI blast [31], Ribosomal Database Project [75], or EzTaxon [76] programs allowed the identification of 12 isolates at the species level, and isolates MD329, MD335 and MD308, which are described as novel taxa in this study, could only be assigned to the *Lachnospiraceae* family. A more precise annotation could be given for the 2 isolates *Clostridium* sp. MD294 and *Clostridium* sp. MD300, respectively as ASF356 and ASF502, since they were obtained from the defined ASF microbial consortium. *Anaerotruncus colihominis* JM4-15 (DSM-28734), *Enterocloster clostridioformis* YL32 (DSM-26114), *Clostridium cocleatum* I50 (DSM-1551), *Escherichia coli* Mt1B1 (DSM-28618) were obtained from DSMZ.

Description of three novel *Lachnospiraceae* strains

The descriptions were performed using Protologger v0.99 [77] and based on 16S rRNA gene sequence analysis and genome sequence analysis including whole proteome-based phylogenomic GBDP (Genome Blast Distance Phylogeny) analysis, percentage of conserved proteins (POCP) and differences in G+C content of DNA.

Description of *Subtilibacillum* gen. nov. *Subtilibacillum* (L. masc./fem. adj. *subtilis*, slender; N.L. neut. n. *bacillum*, rod; N.L. neut. n. *Subtilibacillum*, a slender rod-shaped bacterium). Based on 16S rRNA gene sequence similarity, the closest relative was *Kineothrix alysoides* KX356505 (90.4%). POCP analysis confirmed that strain MD335 represents a distinct genus as all POCP values to close relatives were below 50%. GTDB-Tk supported the placement of strain MD335 within a novel genus predicted metagenomically as 'GCF_000403335.2'. No antibiotic resistance genes were identified within the genome and the G+C content of genomic DNA is 43.7 mol%.The type species is *Subtilibacillum caecimuris*.

Description of *Subtilibacillum caecimuris* sp. nov. *Subtilibacillum caecimuris* (L. n. *caecum*, caecum: L. n. *muris*, mouse; N.L. gen. n. *caecimuris*, from the caecum of a mouse). The cells are rods and strictly anaerobic. The species contains at least 297 CAZymes, however only starch was suggested as a carbon source. KEGG analysis identified pathways for acetate production from acetyl-CoA (EC:2.3.1.8, 2.7.2.1), propionate production from propanoyl-CoA (EC:2.3.1.8, 2.7.2.1), sulfide and L-serine utilized to produce L-cysteine and acetate (EC:2.3.1.30, 2.5.1.47), L-glutamate production from ammonia via L-glutamine (EC:6.3.1.2, 1.4.1.-), and folate biosynthesis from 7,8-dihydrofolate (EC:1.5.13). This novel species was most commonly identified within mouse gut samples (36.9%), although sub-dominant at 0.35% mean relative abundance.

Description of *Longibacillum* gen. nov. *Longibacillum* (L. masc. adj. *longus*, long; N.L. neut. n. *bacillum*, rod; N.L. neut. n. *Longibacillum*, a long rod-shaped bacterium). ANI values to all close relatives were below 95%, and the best match based on 16S rRNA gene sequence similarity was *Roseburia intestinalis* AJ312385 (91.01%). POCP analysis and GTDB-Tk confirmed the creation of a novel genus, placing strain MD329 within the metagenomically predicted genus 'CAG-41'. No antibiotic resistance genes were identified within the genome

and the G +C content of genomic DNA is 39.5 mol%. The type species is *Longibacillum caecimuris*.

Description of *Longibacillum caecimuris* sp. nov. *Longibacillum caecimuris* (L. n. *caecum*, caecum: L. n. *muris*, mouse; N.L. gen. n. *caecimuris*, from the caecum of a mouse). The cells are long rods and strictly anaerobic. Within the genome, 186 CAZymes were identified along with the predicted utilization of starch. KEGG analysis identified pathways for acetate production from acetyl-CoA (EC:2.3.1.8, 2.7.2.1), propionate production from propanoyl-CoA (EC:2.3.1.8, 2.7.2.1), and L-glutamate production from ammonia via L-glutamine (EC:6.3.1.2, 1.4.1.-). This novel species was most commonly identified within mouse gut samples (36.2%), although sub-dominant at 0.53% mean relative abundance.

Description of *Irregularicoccus* gen. nov. *Irregularicoccus* (L. masc./fem. adj. *irregularis*, irregular; N.L. masc. n. *coccus*, coccus from Gr. masc. n. *kokkos*, grain; N.L. masc. n. *Irregularicoccus*, an irregular coccus-shaped bacterium). Strain MD308 was identified as a distinct genus to its closest relative, *Ruminococcus gnavus* X94967 (95.6%), based on 16S rRNA gene sequence similarity since GTDB-Tk was unable to match the input genome to that of a previously sequenced genome via FastANI and POCP values were below 50%. No antibiotic resistance genes were identified within the genome and the G +C content of genomic DNA is 42.77 mol%. The type species of this proposed genus is *Irregularicoccus caecimuris.*

Description of *Irregularicoccus caecimuris* sp. nov. *Irregularicoccus caecimuris* (L. n. *caecum*, caecum: L. n. *muris*, mouse; N.L. gen. n. *caecimuris*, from the caecum of a mouse). The cells are rods that separate into coccoid forms, and strictly anaerobic. The number of CAZymes identified within the genome was 226, facilitating the predicted utilization of cellulose and starch as carbon sources. KEGG analysis identified pathways for acetate production from acetyl-CoA (EC:2.3.1.8, 2.7.2.1), propionate production from propanoyl-CoA (EC:2.3.1.8, 2.7.2.1), sulfide and L-serine utilized to produce L-cysteine and acetate (EC:2.3.1.30, 2.5.1.47), L-glutamate production from ammonia via L-glutamine (EC:6.3.1.2, 1.4.1.-), and folate biosynthesis from 7,8-dihydrofolate (EC:1.5.13). This novel species was most commonly

identified within mouse gut samples (68%), although sub-dominant at 0.69% mean relative abundance.

Culture conditions

Freshly grown cultures of individual bacterial strains were supplemented with 20% glycerol prior cryopreservation at -80°C. Each culture was systematically validated for culture purity and identity by MALDI-TOF. Culture media and material were introduced in the anaerobic chamber at least 2 days before use. Anaerobic bacterial strains were grown in GAM, except *Clostridium* sp. MD300, *Irregularicoccus caecimuris* MD308, *Subtilibacillum caecimuris* MD335 and *Longibacillum caecimuris* MD329 in M2GSC, and *A. colihominis* JM4-15 in Bifidobacterium medium. For mouse colonization and absolute quantification of bacteria, a single colony of each of the 15 bacterial strains was grown and amplified at 37°C. Each bacterial pellet was resuspended in medium, 1 mL was cryopreserved with 10% glycerol, 1 mL was centrifuged and bacterial pellet was stored at -20°C for gDNA extraction, and the rest was used for numeration by dilution plating on agar plates. A frozen mixture of the GM15 bacterial community containing the 15 individual strains at equivalent concentration (6.67E+06 CFU) was prepared to enable easy inoculation.

WGS

DNA samples from the 15 bacterial cultures were prepared for whole-genome sequencing, using the Nextera XT DNA library preparation kit (Illumina, Cat.Nos. FC-XXX, California, USA) according to manufacturer's recommendations. The resulting libraries were checked for their quality using the High-sensitivity DNA chip using the Agilent 2100 Bioanalyzer (Waldbroon, Germany) and quantified using the QuantiFluor One dsDNA kit (Promega). Paired-end (2x300bp) sequencing was performed on a MiSeq sequencer using the "MiSeq v3 kit (600 cycles)" (Illumina, California, USA).

***De novo* genome assembly**

After a quality control with FastQC [78], the paired-end reads were assembled *de novo* using the “A5-miseq” assembly pipeline [79], comprising the following steps: adapter trimming, quality trimming and filtering, error correction, contigging and scaffolding. The 15 *de novo* assemblies resulted in draft genomes composed of few scaffolds (from 30 to 268) with high N50 values (from 13 099 to 943 892). Genomes were then ordered using Mauve [80] and annoted with PGAP of the NCBI database. Default parameters were used for all software tools.

Taxonomic annotation

WGS generated data have been trimmed and quality controlled by AfterQC software [81]. A k-mer counting strategy with the Centrifuge software [29] have been privileged to infer taxonomy, and reads were confronted to the RefSeq complete genome database [30], with bacteria, archaea and viruses domains and the mouse representative genome (taxid 10090), in order to estimate the amount of host DNA contamination and remove it from sequenced data.

Genomic functional analysis

Genes were predicted and translated into protein sequences using Prodigal [82]. Marker genes were searched using the HMM3 package [83]. Predicted proteins sequences of genomes were blasted against the KEGG microbial database [84] which contains 13 millions of proteins sequences and trimmed with following parameters: best-hit with an expected value threshold $< 10^{-5}$. The matrix obtained was consolidated into KEGG orthologs count (KO, which represents a set of genes that have sequence similarities and exert the same function), into KEGG modules (which represent short enzymatic pathways, involving few proteins and doing a targeted function), and into KEGG pathways (i.e. large metabolic pathways). KO were analyzed for their presence absence among genomes. The modules were analyzed for their completion (4 levels: Full, lack 1 enzymes, lack 2 enzymes, absent), and only modules with a score with 3 or 4 were presented and integrated for their KO count. The KEGG pathways were analyzed for their number of related KO count affiliated to them. A list of functions of interest have been designed and their presence among genomes have been analyzed in details

(Additional file 2: Table S1). Because pathways and functions of interest did not have the same number of KO of interest and a different distribution among the genomes, functional data were normalized among each function in order to obtain values that can be comparable. For each function/pathway, the number of different KO was normalized by the total number of KO retrieved. Data were then log-transformed +1. Clusterization of both functions and communities was performed using Euclidian distance and ward's method, and a kmeans clustering was performed in order to define the community clusters.

Identification of specific regions for primers design

NUCmer, a part of the MUMmer package [85], was used to perform pairwise alignment of the 15 genomes. Based on these alignments, PanCake [86] was used with default parameters to identify specific regions of each genome. Specific regions with a length of 200 bp were extracted, meeting the following criteria: GC content between 48 and 52%, distance to a border of a scaffold higher than 300bp, unique in the draft genome. The specificity of each 200bp region was double-checked with BLAST [31] on the 15-genome database and on the NCBI *nr* database. The design of primers on the specific regions was performed by Fluidigm. The primer specificity was checked with BLAST.

Animal experiment

Facility 1: Mice were bred according standardized procedures in the gnotobiology unit of BIOASTER at the ANSES animal facility (Lyon, France), housed in sterilized positive pressure isolators (Noroit) under a 12h light/dark cycle at 22±2°C and 50±30% of humidity, and fed ad libitum with irradiated R03-40 diet (3395 kcal/kg, 25.2% kcal proteins, 61.3% kcal carbohydrates, 13.5% kcal lipids; Safe) and autoclaved water. Irradiated corn-cob granules (Safe) were used as bedding. Sterile enrichment was provided in all cages and was constituted by cotton rolls as nesting material, poplar bricks and a polycarbonate red mouse igloo (Safe). Nesting material and poplar bricks were renewed every two weeks. All breeders were mated by trio (2 females and 1 male) between 8 weeks and 6 months of age, and all mice were

weaned at 4 weeks after birth. C57BL/6J SOPF mice were obtained from Charles River Lab. The fecal samples used for the *in silico* design of the initial metagenome were collected in house from four 2-month-old littermates housed in different cages from weaning at 3 weeks old. C57BL/6J GF mice were produced in-house by aseptic hysterectomy of a C57BL/6J SOPF female, and neonates were fostered on C3H GF mothers (CDTA). Axenic status was assessed weekly by gram staining and cultures of fecal suspension on solid and liquid media. GM15 founders were 8-week-old C57BL/6J GF mice colonized by oral gavage with 215 µL of the fresh frozen GM15 bacterial community, twice at 48h interval. GM15 microbiota composition was analyzed by qPCR microfluidic assay from feces collected at 6-week-old. Alternative diet R04-40 (3339 kcal/kg, 19.3% kcal proteins, 72.4% kcal carbohydrates, 8.4% kcal lipids; Safe) was given at 8-week-old GM15 mice for 4 weeks. FMT was done by oral gavage with a suspension of fresh fecal pellets administered to 7-week-old C57BL/6J GF mice, twice at 48h interval. For undernutrition experiments, GM15 and SOPF male mice were bred and randomly assigned at day 21 after birth to be given either the above R03-40 diet or a custom-made low-protein diet (3500 kcal/kg, 4.7% kcal proteins, 90.1% kcal carbohydrates, 5.3% kcal lipids, Envigo) for 5 weeks after weaning. Mice were killed by cervical dislocation and biocollections were performed aseptically. All animal procedures were approved by the French MESR and the ANSES/ENVA/UPEC ethics committee (APAFIS#4529-2016022616404045v3; APAFIS#785-2015042819315178v2; APAFIS#18918-2019020118003843v3) and were conducted in accordance with the National and European legislation on protection of animals used for scientific purposes.

Facility 2: C57BL/6J GF mice, bred in Laboratory of Gnotobiology for more than 10 generations, were kept under sterile conditions in positive pressure Trexler-type plastic isolators on sterile Abedd Espe LTE E-002 bedding (Abedd, Germany), exposed to 12h light/dark cycles at 22±2°C temperature and 40%-60% humidity, and supplied with autoclaved tap water and 50 kGy irradiated sterile pellet (breeding diet: SSNIFF mouse breeding fortified diet V1124-300, 3338 kcal/kg, 27% kcal proteins, 61% kcal carbohydrates, 12% kcal lipids) ad libitum. Axenicity was assessed every two-weeks by confirming the absence of bacteria, molds

and yeast by aerobic and anaerobic cultivation of mouse feces and swabs from the isolators in VL (Viande-Levure), Sabouraud-dextrose and meat-peptone broth and subsequent plating on blood, Sabouraud and VL agar plates. C57BL/6J SPF mice were kept in individual ventilated cages (Tecniplast, Italy), exposed to 12h light/dark cycles and fed with the same sterile diet as GF counterparts. Animal procedures were approved by the committee for protection and use of experimental animals of the Institute of Microbiology of the Czech Academy of Science (approval ID: 3/2019). GM15 founders were 8-week-old C57BL/6J GF mice orally gavaged with 150 µL of the fresh frozen GM15 bacterial community, twice at 48h interval. GM15 microbiota composition was analyzed by qPCR microfluidic assay as described for Facility 1. Oligo-MM^{12} gnotobiotic mouse line was established in 2018 [27]. Colonized mice were transferred to an experimental isolator and their offspring were used for the experiments. GM15, Oligo-MM^{12} and SPF mice were bred and randomly assigned at day 21 after birth to be given either the SSNIFF V1124-300 diet (males or females) or a custom-made low-protein diet (3500 kcal/kg, 4.7% kcal proteins, 90.1% kcal carbohydrates, 5.3% kcal lipids, Envigo) (males only) for 5 weeks after weaning. For the measurement of body length mice were briefly anesthetized by isofluran (Piramal Healthcare, UK). Weight was measured trice and the scales (Acculab mini PP201, Sartorius, Germany) were tared between the measurements. Males and females on the breeding diet were sacrificed between 9-11 a.m. without food removal. Males fed the depleted diet were sacrificed between 1-3 p.m. after 5 hours starvation. Mice were killed by cervical dislocation and biocollections were performed aseptically.

gDNA extraction from caecal contents and fecal pellets

GM15, SOPF/SPF mice: Caecal and fecal gDNA were extracted using the DNeasy® PowerLyzer® PowerSoil® Kit (Qiagen) following the manufacturer's instructions with modifications. Samples (approximately 0.1g) were heat-treated at 65°C for 10 min, and 95°C for 10 min, before a double bead beating at 30 Hz for 5 min. 50 µL of DNA were obtained with two consecutive elutions.

Oligo-MM^{12} mice: Fecal samples were collected and frozen at -80°C. Fecal gDNA was extracted using the Nucleospin DNA stool kit (Macherey-Nagel) according to the manufacturer's instructions with the following modification: The initial bead-beating step was performed on TissueLyzer (Quiagen) at 40Hz for 7m:30s. gDNA was eluted with 60 µL of SE buffer.

Quantitative PCR microfluidic assay

In order to quantify specific and global bacteria load per g of caecal or fecal samples (wet weight), qPCR microfluidic assay was performed using respectively specific primers for GM15 and "universal" primers amplifying the genes encoding 16S rRNA from most bacteria groups (Additional file 3: Table S2) [87]. Amplicons generated using these primers range between 60 and 99 base pairs. qPCR microfluidic assays were conducted in 48.48 Dynamic Array^{TM} IFCs for EvaGreen Fast Gene Expression on a Biomark HD (Fluidigm) according to the manufacturer's instructions, with cDNA diluted 100-fold, preamplified with pooled primers, and diluted again 100-fold. Each IFC included triplicate reactions per DNA sample, standards and negative control. Standards were generated by serial dilution of a gDNA extract from pure bacterial cultures of known concentration. The efficiency of each qPCR reaction was calculated based on the slope of standard curves and within the range of 78-107%. An equivolume mixture of standards was used to normalize data between runs. Due to the different individual detection limits of the qPCR assay for each primer, the detection limit for GM15 ranged between 2.73×10^2 and 6.57×10^5 CFU/g (Additional file 3: Table S2).

Quantitative PCR of Bacterial 16S rRNA Genes

Quantitative PCR (qPCR) was performed as described previously [22]. Oligo-MM^{12} strain-specific 16S rRNA primers and hydrolysis probes were synthesized by IDT (Integrated DNA Technologies, USA). Standard curves using linearized plasmids containing the 16S rRNA gene sequence of the individual Oligo-MM^{12} strains were used for absolute quantification of 16S rRNA gene copy numbers of individual strains. 16S rRNA gene copy numbers were normalized

to equal volumes of extracted DNA, assuming that DNA extraction is equally efficient between different samples. PCR reaction of 20 µL contained 0,2 µL of 30 µM working solution of each primer; 0,2 µL of 25 µM working solution of corresponding probe; 6,9 µL H2O; 10 µL of 2x PrimeTime® Gene Expression Master Mix (IDT) and 2,5 µL of gDNA of concentration 2 ng/µL. PCR conditions were 95 °C for 3 min, followed by 45 cycles of 95 °C for 15 s and 60 °C for 1 min with fluorescent measurement. PCR reactions were run on qTOWER^3 G touch (Analytik Jena) and analysed using qPCRsoft (Analytik Jena) software.

Sample preparation for immunophenotyping

For flow cytometry analyses whole blood was collected on EDTA tube. Spleen, thymus, MLN and PP were collected in RPMI (Gibco). Single-cell suspensions were achieved using a 100 µm cell-stainer (Becton Dickinson) and a 5 mL syringe plunger in RPMI supplemented with 2% heat-inactivated fetal bovine serum (Sigma) and 100 µg/mL DNASE1 (Roche). Cells were then spun at 400xg for 5 min at room temperature. Medium was discarded and cells were washed using 5 mL of supplemented medium. For whole blood, spleen and thymus samples, red blood cells were lysed by resuspension in 1 mL PharmLyse 1X (Becton Dickinson) for 10 min. Cells were then spun at 400xg for 5 min at room temperature. Lysing solution was discarded and cells were washed using 2 mL of PBS (Gibco). Cells were pelleted a second time and resuspended in PBS supplemented with 2% heat-inactivated fetal bovine serum (Sigma). Numeration and viability were determined using Propidium Iodide marker exclusion and MACSQUANT Flow cytometer (Miltenyi). Cells were then resuspended to a working concentration of 10^6 cells / tube for organs and 100 µL / tube for whole blood, and analyzed by flow cytometry.

Whole blood was collected on dry Eppendorf tube for sera analysis. Sera were obtained by centrifugation 2000xg for 15 min at 4°C and stored at -20°C before Luminex and ELISA analyses. Feces were collected in Eppendorf low-binding tubes and stored at -80°C before Luminex analysis. Feces supernatant was obtained by disrupting 100 mg feces in 1mL PBS-Protease Inhibitor 1X (Sigma) using Lysing Matrix E Tube (MP Biomedicals) and Fast Prep

homogenizer (MP Biomedicals). Samples were spun at 8000xg for 15 min at 4°C and supernatants were collected for IgA Luminex analysis.

Flow Cytometry

10^6 cells or totality of cells for some of PP samples were stained for surface markers. Leukocytes were stained using anti-CD3 BV421 (clone 145-2C11) from Becton Dickinson, and anti-CD45 Viogreen (clone30F11), anti-CD4 PE (clone REA604), anti-CD8a PE Vio615 (clone REA601), anti-CD45 R/B220 PE Vio770 (clone RA3-6B2), anti-CD335 APC (NKp46) (clone 29A1.4.9) and anti-CD11b APC Vio770 (clone REA592) or anti-CD11c APC Vio770 (clone REA754) from Miltenyi Biotec Gmbh. Viable cells were selected using Zombie Green Fixable Viability (Biolegend). T cells were identified as CD45+, CD3+ and CD4+ or CD8+ cellsB cells were identified as CD45+, CD3-, CD45 R/B220 + cells. NK cells were identified as CD45+, CD3-, CD45 R/B220-, NKp46+ cells. Monocytes were identified as CD45+, CD3-, CD45 R/B220-, CD11b+ cells in spleen, thymus and whole blood samples. Dendritic cells were identified as CD45+, CD3-, CD45 R/B220-, CD11c+ cells in spleen, PP and MLN samples. Cells were analyzed using a MACSQuant Ten Flow cytometer (Miltenyi) and raw data were analyzed using FlowJo software (Tree Star, Becton Dickinson). CD45+ cell count were normalized by performing the analysis on 1 M of viable cells stained. For CD45+ cell count comparison in PP, CD45+ cell count were performed on 1 M of viable cells stained when possible and on total viable cells stained when less than 1 M cells were isolated, thus no statistical analysis has been performed on this data. Data normalization was not possible for whole blood sample, thus CD45+ cell count comparison has not been performed for this compartment. For frequency results, data are represented as a percentage of CD45+ cells for all organs.

Metabolic Panel, Ig and Cytokines Luminex

Serum concentrations of Metabolic Panel (Ghrelin, Glucagon, Insulin and Leptin) were determined using the Mouse Metabolic Magnetic Bead Panel Milliplex MAP kit (Millipore).

Samples were not diluted, and assay was performed according to the manufacturer's instructions. Serum concentrations of Ig Panel (IgA, IgG1, IgG2a, IgG2b; IgG3, IgM, IgE) and IgA in feces supernatant were determined using the Mouse Immunoglobulin Isotyping Magnetic Bead Panel Milliplex MAP kit (Millipore) and Mouse IgE Single Plex Magnetic Bead Milliplex MAP kit (Millipore). Samples were diluted 1:12500 (IgA, IgG1, IgG2a, IgG2b; IgG3, IgM), 1:100 (IgE), and 1:100 (IgA in feces supernatant). Assays were performed according to the manufacturer's instructions. Serum concentrations of Cytokines Panel (IL-1b, IL-10, IL-12p70, IL-17a, IL-17f, IL-22) were determined using the Mouse Th17 Magnetic Bead Panel Milliplex MAP kit (Millipore). Samples were not diluted and assay was performed according to the manufacturer' instructions. Samples were assayed in monoplicate. The known intra technical error (%CV) per assay was 7% for Insulin, 8% for Glucagon, 6% for Leptin, 15% for Ghrelin, 10% for IgA, 6% for IgG1, 8% for IgG2a, 7% for IgG2b, 5% for IgG3, 5% for IgM, 2% for IL-1b, 3% for IL-10, 2% for IL-12p70, 3% for IL-17a, 3% for IL-17f, and 3% for IL-22.

Corticosterone, IGF-1, IGFBP-3 and total IgE ELISAs

Serum concentrations of Corticosterone were determined using the Corticosterone ELISA kit (Abnova). Samples were diluted 1:50, and assay was performed according to the manufacturer' instructions. Serum concentrations of IGF-1 and IGFBP-3 were determined using the Mouse/Rat IGF-1 Quantikine ELISA kit (R&D Systems) and IGFBP-3 DuoSet ELISA kit (R&D Systems), respectively. Samples were diluted 1:500, and assay was performed according to the manufacturer' instructions. Serum concentrations of total IgE were quantified with BD OptEIA™ Mouse IgE ELISA Set (BD Biosciences, San Chose, Canada) with samples diluted 1:100 according to manufacturer's instructions. Samples were assayed in monoplicate.

Sample preparation for metabophenotyping

Polar metabolites preparation

It is known that the quantification of some plasma metabolites, such as tryptophan and tyrosine, is biased since they bind to albumin, a highly abundant protein in plasma [88]. In

addition, protein precipitation methods with organic solvents can induce loss of volatile metabolites and overlay of residual broad resonances of lipids with some polar metabolites [89]. Thus, the polar and non-polar metabolites extraction from the same plasma sample was adapted according to previously described sequential approaches [90, 91]. First, we deproteinized the plasma samples by acidified ultrafiltration in order to increase desorption yields of aromatic amino acids and then, quantify the polar metabolites. The concentration of the formic acid was optimized to allow desorption of the metabolites like tryptophan from plasma albumin. In practice, frozen mice plasma samples were thawed in thermoshaker Eppendorf (10 min, 10°C and 1000 rpm). The entire amount of plasma (about 180 µL) was filtered using 0.2 µm centrifugal tube from VWR (5 min, 10°C, 10000xg). Next, the lipoproteins removal was performed by mixing 150 µL of filtered plasma with 50 µL of milli-Q water and 10 µL of deuterated formic acid (0.1% final concentration) in a clean 10 kDa cut-off ultracentrifugation tube (VWR) using thermoshaker Eppendorf (10 min, 10°C, 750 rpm), and then by centrifugation (30 min, 10°C, 10000xg, soft ramp). Deuterated formic acid was used instead of protonated form to decrease the exogenous NMR signal and allow the quantification of the endogenous formiate. Clean 10 kDa cut-off ultracentrifugation tubes were prepared by recovering filters from tubes, transferring them into a 250 mL Duran bottle plunged in milli-Q water and then sonicated in a bath for 10 min, repeated five times. After the last step, the 10 kDa cut-off ultracentrifugation filters could be stored in milli-Q water for at least 3 months. Just before use, nitrogen stream was used to discard any traces of milli-Q water. We observed that this ultrasonication procedure removes better the residual glycerol than supplier's protocol and gives higher yields of ultrafiltered plasma. Indeed, glycerol was completely discarded in the ultrasonicated tubes (N = 5; average = under detection limit), while it was still present after centrifugation following washes with either sodium hydroxide 0.05N followed by 4 washes with milli-Q water (N = 5; average = 0.02 mM; standard deviation = 0.02 mM), or ethanol 70% followed by 4 washes with milli-Q water (N = 5; average = 0.05 mM; standard deviation = 0.01 mM), or 5 control washes with milli-Q water (N = 5; average = 0.02 mM; standard deviation = 0.01 mM). In addition, we observed that the use of ethanol contributed to contamination since

traces of ethanol remain. Finally, regarding the mechanical properties of the filters, we also observed that after 5 washes and centrifugations at 10000xg, filters collapsed during plasma filtration.

Vortexed 10 kDa-filtered plasma samples (about 135 µL) were transferred in a 0.5 mL 96-well plate (Agilent) and mixed on thermoshaker Eppendorf (1.5 min, 10°C, 650 rpm) with 45 µL of internal standard solution DSS-d6 (1.54 mM), which also contains the pH-reference standard DFTMP (4 mM). The internal standard solution DSS-d6 was prepared with phosphate buffer (0.6 M, 60:40 v/v H_2O:D_2O, pH=7.4). Finally, 155 µL of the resulting sample solutions were transferred in 3 mm SampleJet NMR tubes. Since the DSS-d6 solution might be unstable during long time storage (hydroscopic properties, trimethylsilyl fragment degradation, etc.), the DSS-d6 concentration was calibrated by ^{1}H NMR using sodium succinate dibasic hexahydrate standard solution, a compound with better stability properties, in order to guarantee data accuracy. This protocol was systematically applied including for blank samples, which were prepared by replacing the plasma by Milli-Q water and for quality controls (n=7), which were prepared using commercially available mouse plasma.

Non-polar metabolites extraction after ultrafiltration

Then, the lipoproteins on the 10 kDa filters were further diluted with 150 µL phosphate buffer solution (1 M, pH=7.4), mixed on thermoshaker Eppendorf (10 min, 10°C, 750 rpm), transferred in clean Eppendorf tubes and extracted with 400 µL methanol-dichlormethan (1:2 v/v). Samples were centrifuged (5 min, 10°C, 10000xg) for better phase separation. The dichlormethan layer was transferred in clean Eppendorf tubes and the aqueous phase was extracted again with dichlormethan. The pooled organic phase was evaporated under nitrogen stream. The dry lipidic residue was dissolved with 200 µL deuterated chloroform containing 0.03% TMS internal standard and 155 µL of resulting solution was transferred in 3 mm SampleJet NMR tube. The TMS concentration was calibrated by NMR using 1,3,5-tritertbutylbenzen standard solution and it was found to be 0.435 mM.

Metabolites analysis and quantification

The 1D ^{1}H NMR spectra were acquired at 298 K with 600 MHz Ascend (Avance III HD) spectrometer from Bruker equipped with a 5 mm QCI cryoprobe. All samples were stored at 6°C in the SampleJet autosampler. Polar metabolites were analyzed using *noesygppr1d* pulse sequence. For each spectrum, 128 scans were collected into 32k data points within 14 ppm spectroscopic width and a recycling delay of 4 s. The mixing time was calibrated to 50 ms and the acquisition time was 3.9 s. The non-polar metabolites NMR spectra were acquired using *zg30* pulse sequence. The spectra were recording using 256 scans, into 32k data point and a spectroscopic width of 20 ppm. The relaxation delay was 4 s. The FIDs were zero-filled to 64k points and Fourier transformed using 0.3 Hz exponential line-broadening function. All spectra were aligned to DSS-d6 and TMS respectively internal standard. The concentrations of the polar and non-polar metabolites were quantified using Chenomx NMR suite 8.6. The Chenomx software was applied also for spectra binning of 10^{-3} ppm width for each bin. The triacyl glycerol (TAG), phosphatidylcholine (PC), lysophosphatidylcholine (LysoPC), sphingomyelin (SM), free cholesterol (FC) and cholesterol ester (EC) quantification an in-house lipid database within Chenomx was built with authentic lipid standards. The lipids database spectra were recorded using the same parameters as described above for non-polar metabolites.

Metabolomics data analysis

Discriminant analyses were performed using the partial least square (PLS-DA) algorithm to extract metabolomics signatures [92, 93]. A variable selection algorithm based on Elastic-Net was used to improve model performance by selecting most significant metabolic signatures that explain the groups (GF, GM15, SOPF). The statistical performances of the regression models were assessed using the balanced error rate with and without cross-validation (E2 and CV-E2) and permutation tests. Permutation tests consisted in building the null distribution of the balanced error rate E2 by randomly permuting observations. Regression models were thus challenged by testing if the cross-validation error rate CV-E2 is significantly different from the null distribution with a p-value < 0.05. Metabolites involved in the cross-validated signatures

were ranked by order of importance in the PLS-DA model using their VIP (variable importance in projection) scores. The biplot allows projecting onto the two first components, the samples and the metabolites that significantly discriminate each sample groups. Metabolites that are positively correlated (or positively contribute) to a sample group will point to the direction of this group. They will point to the reverse direction for a negative correlation.

Statistics

Reproductive performance and body growth were analyzed respectively by 1-way and 2-way ANOVA. Phenotyping data impacted by age, filial generation or sex, were analyzed by the F-test for multiple linear regressions (R v3.4.2), otherwise by 1-way ANOVA and Tukey's multiple comparison parametric test or Kruskal-Wallis and Dunn's multiple comparison non-parametric test after D'Agostino et Pearson test for data set normality assessment (GraphPad Prism v7 and v8). PCA for phenotyping analysis was performed using R v3.4.2 and the ade4 package [94].

Supplementary information

Additional file 1: Fig. S1. Distribution of bacterial families among the C57BL/6J SOPF mice used to design the GM15 community and morphological features of the GM15 strains. (TIF 2807 kb)

Additional file 2: Table S1. KEGG clusters. (XLSX 142 kb)

Additional file 3: Table S2. GM15 strains-specific primers. (XLSX 12 kb)

Additional file 4: Fig. S2. *In vivo* experimental design. (TIF 855 kb)

Additional file 5: Fig. S3. Assessment of gut microbiota stability of GM15 founders, and of reproducibility between fecal and caecal samples of individual mice. (TIF 918 kb)

Additional file 6: Fig. S4. Immune cell populations profiling. (TIF 476 kb)

Additional file 7: Table S3. Polar metabolites and lipids concentration in plasma samples. (XLSX 192 kb)

Additional file 8: Fig. S5. PCA based on binned NMR spectra. (TIF 1374 kb)

Additional file 9: Fig. S6. Measurements of several organs after nutritional challenge. (TIFF 925 kb)

Additional file 10: Fig. S7. Assessment of gut microbiota reproducibility in GM15 and SOPF/SPF mice in 2 animal facilities, and Oligo-MM^{12} gut microbiota stability in facility 2. (TIFF 1157 kb)

Additional file 11: Fig. S8. Measurements of organs weight of animals from facility 2. (TIFF 955 kb)

Additional file 12: Fig. S9. Immune phenotype and metabolic profile of animals from facility 2. (TIFF 916 kb)

Abbreviations

ASF: Altered Schaedler flora; BD: Breeding diet; bp: Base pair; CFU: colony forming units; CNA: Colistin and naladixic acid; DD: Depleted diet; FMT: Fecal microbiota transplantation; GAM: Gifu anaerobic medium; gDNA: Genomic deoxyribonucleic acid; GF: Germ-free; IFC: Integrated fluidic circuit; KO: KEGG orthology; MLN: mesenteric lymph nodes; MRS: Man Rogosa Sharpe medium; OTU: Operational taxonomic unit; PCA: Principal component analysis; PP: Peyer's patches; NMR: Nuclear magnetic resonance; qPCR: Quantitative polymerase chain reaction; SEM: Standard error of the mean; SOPF: Specific and opportunistic pathogen-free; SPF: Specific pathogen-free; WGS: Whole genome sequencing

Acknowledgments

We thank Julie Henry, Leanne Goncalves, Christelle Boisse and Gustavo Stadthagen Gomez for help with bacterial cultures and gram staining, Cécile Chauvel, May Taha, Joséphine Abi Ghanem, and Adrien Villain for help with biostatistics, and Vincent Thomas, Gianfranco Grompone, Laurent Beloeil and Alain Troesch for valuable comments and discussions, and Jaroslava Valterová and Šárka Maisnerová for technical assistance. This work was supported by the French Government as part of the Programme des Investissements d'Avenir (grant N°ANR-10-AIRT-03). Research in F.L. lab was supported by ENS de Lyon, CNRS, the FINOVI

foundation and the Fondation pour la Recherche Médicale (Equipe FRM DEQ20180339196). M.S. acknowledges the support of 18-07015Y of the Czech Science Foundation and EMBO Installation grant.

Author contributions

M.D., F.L. and A.T. conceived the project, analyzed, interpreted and integrated all the data. M.D. and F.L. wrote the manuscript. M.D. prepared figures. L.B. and J.Y. achieved *in silico* design. M.D. performed bacteria isolation and identification, gDNA extraction, developed the qPCR microfluidic assay and analyzed macroscopic phenotyping data. A.S. carried out WGS, C.E. identified specific regions for primers design, and A.M. performed taxonomic annotation and functional bioinformatic analyses. P.B., H.D., M.D, T.N., D.S. and M.S. performed animal experiments. B.S. provided the Oligo-MM^{12} consortium. T.N. performed the Oligo-MM^{12} related gDNA extraction and consortium analysis with help of B.S. C.C., A.D., S.P. and M.S. performed the immunophenotyping, analyzed and interpreted data. A.B. and D.A.O. performed the metabophenotyping, analyzed and interpreted data. M.S. helped design the diet-induced stunting protocol. F.D.V. performed, analyzed and contributed to the text and figures related to the stunting model experiments. A.L.B. provided technical support during the stunting model experiments. All authors read and approved the final manuscript.

Competing interests

The authors declare that they have no competing interests.

Data availability

The 15 assembled genomes and the corresponding sequencing reads have been deposited in the DDBJ/ENA/GenBank data banks and the Sequence Read Archive respectively, under the BioProject number PRJNA551571 [32]. NMR raw data will be accessible at the NIH Common Fund's National Metabolomics Data Repository (supported by NIH grant, U01-DK097430) website, the Metabolomics Workbench, https://www.metabolomicsworkbench.org.

References

1. Lynch SV, Pedersen O. The Human Intestinal Microbiome in Health and Disease. NEJM. 2016;375:2369-79.
2. Knight R, Callewaert C, Marotz C, Hyde ER, Debelius JW, McDonald D, Sogin ML. The Microbiome and Human Biology. Annu Rev Genomics Hum Genet. 2017;18:65-86.
3. Bik EM. The Hoops, Hopes, and Hypes of Human Microbiome Research. Yale J Biol Med. 2016;89:363-73.
4. Leulier F, MacNeil LT, Lee WJ, Rawls JF, Cani PD, Schwarzer M, Zhao L, Simpson SJ. Integrative Physiology: At the Crossroads of Nutrition, Microbiota, Animal Physiology, and Human Health. Cell metab. 2017;25:522-34.
5. Nguyen TLA, Vieira-Silva S, Liston A, Raes J. How informative is the mouse for human gut microbiota research? Dis Model Mech. 2015;8:1-16.
6. Mähler Convenor M, Berard M, Feinstein R, Gallagher A, Illgen-Wilcke B, Pritchett-Corning K, Raspa M. FELASA recommendations for the health monitoring of mouse, rat, hamster, guinea pig and rabbit colonies in breeding and experimental units. Lab Anim. 2014;48:178-92.
7. Mamantopoulos M, Ronchi F, Van Hauwermeiren F, Vieira-Silva S, Yilmaz B, Martens L, Saeys Y, Drexler SK, Yazdi AS, Raes J, Lamkanfi M, McCoy KD, Wullaert A. Nlrp6- and ASC-Dependent Inflammasomes Do Not Shape the Commensal Gut Microbiota Composition. Immunity. 2017;47:339-48.
8. Ussar S, Griffin NW, Bezy O, Fujisaka S, Vienberg S, Softic S, Deng L, Bry L, Gordon JI, Kahn CR. Interactions between Gut Microbiota, Host Genetics and Diet Modulate the Predisposition to Obesity and Metabolic Syndrome. Cell Metab. 2015;22:516-30.
9. Franklin CL, Ericsson AC. Microbiota and reproducibility of rodent models. Lab Anim (NY). 2017;46(4):114-122.

10. Mooser C, Gomez de Agüero M, Ganal-Vonarburg SC. Standardization in host-microbiota interaction studies: challenges, gnotobiology as a tool, and perspective. Curr Opin Microbiol. 2018;44:50-60.

11. Laukens D, Brinkman BM, Raes J, De Vos M, Vandenabeele P. Heterogeneity of the gut microbiome in mice: guidelines for optimizing experimental design. FEMS Microbiol Rev. 2016;40:117-32.

12. Stappenbeck TS, Virgin HW. Accounting for reciprocal host-microbiome interactions in experimental science. Nature. 2016;534:191-9.

13. Clavel T, Lagkouvardos I, Blaut M, Stecher B. The mouse gut microbiome revisited: From complex diversity to model ecosystems. Int J Med Microbiol. 2016;306:316-327.

14. McCoy KD, Geuking MB, Ronchi F. Gut Microbiome Standardization in Control and Experimental Mice. Curr Protoc Immunol. 2017;117:1-13.

15. Ley RE, Bäckhed F, Turnbaugh P, Lozupone CA, Knight RD, Gordon JI. Obesity alters gut microbial ecology. Proc Natl Acad Sci U S A. 2005;102:11070-5.

16. Xiao L, Feng Q, Liang S, Sonne SB, Xia Z, Qiu X, Li X, Long H, Zhang J, Zhang D, Liu C, Fang Z, Chou J, Glanville J, Hao Q, Kotowska D, Colding C, Licht TR, Wu D, Yu J, Sung JJ, Liang Q, Li J, Jia H, Lan Z, Tremaroli V, Dworzynski P, Nielsen HB, Bäckhed F, Doré J, Le Chatelier E, Ehrlich SD, Lin JC, Arumugam M, Wang J, Madsen L, Kristiansen K. A catalog of the mouse gut metagenome. Nat Biotechnol. 2015;33:1103-8.

17. Lane-Petter W. Provision of pathogen-free animals. Proc R Soc Med. 1962;55:253–256.

18. Macpherson AJ, McCoy KD. Standardised animal models of host microbial mutualism. Mucosal Immunol. 2015;8:476-86.

19. Lagkouvardos I, Pukall R, Abt B, Foesel BU, Meier-Kolthoff JP, Kumar N, Bresciani A, Martínez I, Just S, Ziegler C, Brugiroux S, Garzetti D, Wenning M, Bui TP, Wang J, Hugenholtz F, Plugge CM, Peterson DA, Hornef MW, Baines JF, Smidt H, Walter J, Kristiansen K, Nielsen HB, Haller D, Overmann J, Stecher B, Clavel T. The Mouse Intestinal

Bacterial Collection (miBC) provides host-specific insight into cultured diversity and functional potential of the gut microbiota. Nat Microbiol. 2016;1:16131.

20. Clavel T, Gomes-Neto JC, Lagkouvardos I, Ramer-Tait AE. Deciphering interactions between the gut microbiota and the immune system via microbial cultivation and minimal microbiomes. Immunol Rev. 2017;279:8-22.

21. Wymore Brand M, Wannemuehler MJ, Phillips GJ, Proctor A, Overstreet AM, Jergens AE, Orcutt RP, Fox JG. The Altered Schaedler Flora: Continued Applications of a Defined Murine Microbial Community. ILAR Journal. 2015;56:169-78.

22. Brugiroux S, Beutler M, Pfann C, Garzetti D, Ruscheweyh HJ, Ring D, Diehl M, Herp S, Lötscher Y, Hussain S, Bunk B, Pukall R, Huson DH, Münch PC, McHardy AC, McCoy KD, Macpherson AJ, Loy A, Clavel T, Berry D, Stecher B. Genome-guided design of a defined mouse microbiota that confers colonization resistance against Salmonella enterica serovar Typhimurium. Nature Microbiology. 2016;2:16215.

23. Schaedler RW, Dubos R, Costello R. J Exp Med. 1965;122:77-83.

24. Norin E, Midtvedt T. Intestinal microflora functions in laboratory mice claimed to harbor a "normal" intestinal microflora. Is the SPF concept running out of date? Anaerobe. 2010;16:311-3.

25. Uchimura Y, Wyss M, Brugiroux S, Limenitakis JP, Stecher B, McCoy KD, Macpherson AJ. Complete Genome Sequences of 12 Species of Stable Defined Moderately Diverse Mouse Microbiota 2. Genome Announc. 2016;4.

26. Garzetti D, Brugiroux S, Bunk B, Pukall R, McCoy KD, Macpherson AJ, Stecher B. High-Quality Whole-Genome Sequences of the Oligo-Mouse-Microbiota Bacterial Community. Genome Announc. 2017;5.

27. Eberl C, Ring D, Münch PC, Beutler M, Basic M, Slack EC, Schwarzer M, Srutkova D, Lange A, Frick JS, Bleich A, Stecher B. Reproducible Colonization of Germ-Free Mice With the Oligo-Mouse-Microbiota in Different Animal Facilities. Front Microbiol. 2020;10:2999.

28. Yilmaz B, Mooser C, Keller I, Li H, Zimmermann J, Bosshard L, Fuhrer T, Gomez de Agüero M, Trigo NF, Tschanz-Lischer H, Limenitakis JP, Hardt WD, McCoy KD, Stecher B,

Excoffier L, Sauer U, Ganal-Vonarburg SC, Macpherson AJ. Long-term evolution and short-term adaptation of microbiota strains and sub-strains in mice. Cell Host Microbe. 2021;29(4):650-663.

29. Kim D, Song L, Breitwieser FP, Salzberg SL. Centrifuge: rapid and sensitive classification of metagenomic sequences. Genome Res. 2016;26:1721-9.

30. O'Leary NA, Wright MW, Brister JR, Ciufo S, Haddad D, McVeigh R, Rajput B, Robbertse B, Smith-White B, Ako-Adjei D, Astashyn A, Badretdin A, Bao Y, Blinkova O, Brover V, Chetvernin V, Choi J, Cox E, Ermolaeva O, Farrell CM, Goldfarb T, Gupta T, Haft D, Hatcher E, Hlavina W, Joardar VS, Kodali VK, Li W, Maglott D, Masterson P, McGarvey KM, Murphy MR, O'Neill K, Pujar S, Rangwala SH, Rausch D, Riddick LD, Schoch C, Shkeda A, Storz SS, Sun H, Thibaud-Nissen F, Tolstoy I, Tully RE, Vatsan AR, Wallin C, Webb D, Wu W, Landrum MJ, Kimchi A, Tatusova T, DiCuccio M, Kitts P, Murphy TD, Pruitt KD. Reference sequence (RefSeq) database at NCBI: current status, taxonomic expansion, and functional annotation. Nucleic Acids Res. 2016;44:D733-45.

31. Altschul SF, Gish W, Miller W, Myers EW, Lipman DJ. Basic local alignment search tool. J Mol Biol. 1990;215:403-10.

32. Elie C, Mathieu A, Saliou A, Villain A, Darnaud M, Leulier F, Tamellini A. Draft Genome Sequences of 15 Bacterial Species Constituting the Stable Defined Intestinal Microbiota of the GM15 Gnotobiotic Mouse Model. Microbiol Resour Announc. 2020;9(35):e00686-20.

33. Plaza-Diaz J, Ruiz-Ojeda FJ, Gil-Campos M, Gil A. Mechanisms of action of probiotics. Adv Nutr. 2019;10:S49-66.

34. Feldman-Salit A, Hering S, Messiha HL, Veith N, Cojocaru V, Sieg A, Westerhoff HV, Kreikemeyer B, Wade RC, Fiedler T. Regulation of the activity of lactate dehydrogenases from four lactic acid bacteria. J Biol Chem. 2013;288:21295-306.

35. Galperin MY. Genome diversity of spore-forming Firmicutes. Microbiol Spectr. 2013;1.

36. Browne HP, Forster SC, Anonye BO, Kumar N, Neville BA, Stares MD, Goulding D, Lawley TD. Culturing of ‘unculturable’ human microbiota reveals novel taxa and extensive sporulation. Nature. 2016;533:543-46.

37. Mukhopadhya I, Moraïs S, Laverde-Gomez J, Sheridan PO, Walker AW, Kelly W, Klieve AV, Ouwerkerk D, Duncan SH, Louis P, Koropatkin N, Cockburn D, Kibler R, Cooper PJ, Sandoval C, Crost E, Juge N, Bayer EA, Flint HJ. Sporulation capability and amylosome conservation among diverse human colonic and rumen isolates of the keystone starch-degrader Ruminococcus bromii. Environ Microbiol. 2018;20:324-36.

38. Pearson JP, Brownlee IA. The interaction of large bowel microflora with the colonic mucus barrier. Int J Inflam. 2010;2010:321426.

39. Macy JM, Ljungdahl LG, Gottschalk G. Pathway of succinate and propionate formation in Bacteroides fragilis. J Bacteriol. 1978;134:84-91.

40. Johnson JL, Moore WEC, Moore LVH. Bacteroides Caccae sp.nov., Bacteroides merdae sp.nov., and Bacteroides stercoris sp.nov. isolated from human feces. Int J Sys Bacteriol. 1986;36:499-501.

41. Wannemuehler MJ, Overstreet AM, Ward DV, Phillips GJ. Draft genome sequences of the altered schaedler flora, a defined bacterial community from gnotobiotic mice. Genome Announc. 2014;2.

42. Thompson GR, Trexler PC. Gastrointestinal structure and function in germ-free or gnotobiotic animals. Gut. 1971; 12:230-235.

43. Schwarzer M, Makki K, Storelli G, Machuca-Gayet I, Srutkova D, Hermanova P, Martino ME, Balmand S, Hudcovic T, Heddi A, Rieusset J, Kozakova H, Vidal H, Leulier F. Lactobacillus plantarum strain maintains growth of infant mice during chronic undernutrition. Science. 2016;351:854-7.

44. Yan J, Herzog JW, Tsang K, Brennan CA, Bower MA, Garrett WS, Sartor BR, Aliprantis AO, Charles JF. Gut microbiota induce IGF-1 and promote bone formation and growth. Proc Natl Acad Sci U S A. 2016;113:E7554-63.

45. Chung H, Pamp SJ, Hill JA, Surana NK, Edelman SM, Troy EB, Reading NC, Villablanca EJ, Wang S, Mora JR, Umesaki Y, Mathis D, Benoist C, Relman DA, Kasper DL. Gut immune maturation depends on colonization with a host-specific microbiota. Cell. 2012;149:1578-93.

46. Sjögren YM, Tomicic S, Lundberg A, Böttcher MF, Björkstén B, Sverremark-Ekström E, Jenmalm MC. Influence of early gut microbiota on the maturation of childhood mucosal and systemic immune responses. Clin Exp Allergy. 2009;39:1842-51.

47. Cahenzli J, Köller Y, Wyss M, Geuking MB, McCoy KD. Intestinal microbial diversity during early-life colonization shapes long-term IgE levels. Cell Host Microbe. 2013;14:559-70.

48. Koch MA, Reiner GL, Lugo KA, Kreuk LSM, Stanbery AG, Ansaldo E, Seher TD, Ludington WB, Barton GM. Maternal IgG and IgA antibodies dampen mucosal T helper cell responses in early life. Cell. 2016;165:827-41.

49. Durand A, Audemard-Verger A, Guichard V, Mattiuz R, Delpoux A, Hamon P, Bonilla N, Rivière M, Delon J, Martin B, Auffray C, Boissonnas A, Lucas B. Profiling the lymphoid-resident T cell pool reveals modulation by age and microbiota. Nat Commun. 2018;9:68.

50. Bouskra D, Brézillon Christophe, Bérard M, Werts C, Varona R, Gomperts Boneca I, Eberl G. Lymphoid tissue genesis induced by commensals though NOD1 regulates intestinal homeostasis. Nature. 2008;456:507-10.

51. Kennedy EA, King KY, Baldridge MT. Mouse Microbiota Models: Comparing Germ-Free Mice and Antibiotics Treatment as Tools for Modifying Gut Bacteria. Front Physiol. 2018;9:1534.

52. Tanaka M, Nakayama J. Development of the gut microbiota in infancy and its impact on health in later life. Allergol Int. 2017;66:515-22.

53. Hong SW, O E, Lee JY, Lee M, Han D, Ko HJ, Sprent J, Surh CD, Kim KS. Food antigens drive spontaneous IgE elevation in the absence of commensal microbiota. Sci Adv. 2019;5:eaaw1507.

54. Nicholson JK, Holmes E, Kinross J, Burcelin R, Gibson G, Jia W, Pettersson S. Host-gut microbiota metabolic interactions. Science. 2012;336:1262-7.

55. Cani PD, Knauf C. How gut microbes talk to organs: The role of endocrine and nervous routes. Mol Metab. 2016;5:743-52.

56. Mestdagh R, Dumas ME, Rezzi S, Kochhar S, Holmes E, Claus SP, Nicholson JK. Gut microbiota modulate the metabolism of brown adipose tissue in mice. J Proteome Res. 2012;11:620-30.

57. Claus SP, Tsang TM, Wang Y, Cloarec O, Skordi E, Martin FP, Rezzi S, Ross A, Kochhar S, Holmes E, Nicholson JK. Systemic multicompartmental effects of the gut microbiome on mouse metabolic phenotypes. Mol Syst Biol. 2008;4:219.

58. Org E, Blum Y, Kasela S, Mehrabian M, Kuusisto J, Kangas AJ, Soininen P, Wang Z, Ala-Korpela M, Hazen SL, Laakso M, Lusis AJ. Relationships between gut microbiota, plasma metabolites, and metabolic syndrome traits in the METSIM cohort. Genome Biol. 2017;18:70.

59. Mardinoglu A, Shoaie S, Bergentall M, Ghaffari P, Zhang C, Larsson E, Bäckhed F, Nielsen J. The gut microbiota modulates host amino acid and glutathione metabolism in mice. Mol Syst Biol. 2015;11:834.

60. Trent CM, Blaser MJ. Microbially Produced Acetate: A "Missing Link" in Understanding Obesity? Cell Metab. 2016;24:9-10.

61. He X, Slupsky CM. Metabolic fingerprint of dimethyl sulfone (DMSO2) in microbial-mammalian co-metabolism. J Proteome Res. 2014;13:5281-92.

62. Dorokhov YL, Shindyapina AV, Sheshukova EV, Komarova TV. Metabolic methanol: molecular pathways and physiological roles. Physiol Rev. 2015;95:603-44.

63. Max B, Salgado JM, Rodríguez N, Cortés S, Converti A, Domínguez JM. Biotechnological production of citric acid. Braz J Microbiol. 2010;41:862-75.

64. Santos GA, Moura RF, Vitorino DC, Roman EA, Torsoni AS, Velloso LA, Torsoni MA. Hypothalamic AMPK activation blocks lipopolysaccharide inhibition of glucose production in mice liver. Mol Cell Endocrinol. 2013;381:88-96.

65. Molinaro A, Caesar R, Holm LM, Tremaroli V, Cani PD, Bäckhed F. Host-microbiota interaction induces bi-phasic inflammation and glucose intolerance in mice. Mol Metab. 2017;6:1371-80.

66. Lee YH, Hsu HC, Kao PC, Shiao YJ, Yeh SH, Shie FS, Hsu SM, Yeh CW, Liu HK, Yang SB, Tsay HJ. Augmented Insulin and Leptin Resistance of High Fat Diet-Fed APPswe/PS1dE9 Transgenic Mice Exacerbate Obesity and Glycemic Dysregulation. Int J Mol Sci. 2018;19.

67. Kaplan SA, Cohen P. The somatomedin hypothesis 2007: 50 years later. J Clin Endocrinol Metab. 2007;92:4529-35.

68. Klover P, Hennighausen L. Postnatal body growth is dependent on the transcription factors signal transducers and activators of transcription 5a/b in muscle: a role for autocrine/paracrine insulin-like growth factor I. Endocrinology. 2007;148:1489-97.

69. Luczynski P, McVey Neufeld KA, Oriach CS, Clarke G, Dinan TG, Cryan JF. Growing up in a Bubble: Using Germ-Free Animals to Assess the Influence of the Gut Microbiota on Brain and Behavior. Int J Neuropsychopharmacol. 2016;19.

70. Blanton LV, Barratt MJ, Charbonneau MR, Ahmed T, Gordon JI. Childhood undernutrition, the gut microbiota, and microbiota-directed therapeutics. Science. 2016;352:1533.

71. Gehrig JL, Venkatesh S, Chang HW, Hibberd MC, Kung VL, Cheng J, Chen RY, Subramanian S, et al. Effects of microbiota-directed foods in gnotobiotic animals and undernourished children. Science. 2019;365.

72. Nishimori JH, Newman TN, Oppong GO, Rapsinski GJ, Yen JH, Biesecker SG, Wilson RP, Butler BP, Winter MG, Tsolis RM, Ganea D, Tükel Ç. Microbial amyloids induce interleukin 17A (IL-17A) and IL-22 responses via Toll-like receptor 2 activation in the intestinal mucosa. Infect Immun. 2012;80:4398-408.

73. https://www.biomerieux-industry.com/fr/products/vitek-ms-rapid-identification-microorganisms-mass-spectrometry

74. Edgar RC. 2018. Updating the 97% identity threshold for 16S ribosomal RNA OTUs. Bioinformatics. 2018;34:2371-5.

75. Wang Q, Garrity GM, Tiedje JM, Cole JR. Naive Bayesian classifier for rapid assignment of rRNA sequences into the new bacterial taxonomy. Appl Environ Microbiol. 2007;73:5261-7.

76. Kim OS, Cho YJ, Lee K, Yoon SH, Kim M, Na H, Park SC, Jeon YS, Lee JH, Yi H, Won S, Chun J. Introducing EzTaxon-e: a prokaryotic 16S rRNA gene sequence database with phylotypes that represent uncultured species. Int J Syst Evol Microbiol. 2012;62:716-21.

77. Hitch TCA, Riedel T, Oren A, Overmann J, Lawley TD, Clavel T. Automated analysis of genomic sequences facilitates highthroughput and comprehensive description of bacteria. ISME Commun. 2021;1:16.

78. Andrews S. FastQC: a quality control tool for high throughput sequence data. 2010. Available online at: http://www.bioinformatics.babraham.ac.uk/projects/fastqc

79. Coil D, Jospin G, Darling AE. A5-miseq: an updated pipeline to assemble microbial genomes from Illumina MiSeq data. Bioinformatics. 2015;31:587-9.

80. Darling AE, Tritt A, Eisen JA, Facciotti MT. Mauve Assembly Metrics. Bioinformatics. 2011;27:2756-7.

81. Chen S, Huang T, Zhou Y, Han Y, Xu M, Gu J. AfterQC: automatic filtering, trimming, error removing and quality control for fastq data. BMC Bioinformatics. 2017;18:80.

82. Hyatt D, Chen GL, Locascio PF, Land ML, Larimer FW, Hauser LJ. Prodigal: prokaryotic gene recognition and translation initiation site identification. BMC Bioinformatics. 2010;11:119.

83. Finn RD, Clements J, Arndt W, Miller BL, Wheeler TJ, Schreiber F, Bateman A, Eddy SR. HMMER web server: 2015 update. Nucleic Acids Res. 2015;43:W30-8.

84. Kanehisa M, Sato Y, Kawashima M, Furumichi M, Tanabe M. KEGG as a reference resource for gene and protein annotation. Nucleic Acids Res. 2016;44:D457-62.

85. Delcher AL, Salzberg SL, Phillippy AM. Using MUMmer to identify similar regions in large sequence sets. Curr Protoc Bioinformatics. 2003;Chapter 10:Unit 10.3.

86. Ernst C, Rahmann S. PanCake: a data structure for pangenomes. German conference on bioinformatics 2013. 2013:35-45.

87. Packey CD, Shanahan MT, Manick S, Bower MA, Ellermann M, Tonkonogy SL, Carroll IM, Sartor RB. Molecular detection of bacterial contamination in gnotobiotic rodent units. Gut Microbes. 2013;4:361-70.

88. Spector AA. Fatty acid binding to plasma albumin. J Lipid Res. 1975;16:165-79.

89. Nagana Gowda GA, Raftery D. Quantitating metabolites in protein precipitated serum using NMR spectroscopy. Anal Chem. 2014;86:5433-40.

90. Tiziani S, Emwas AH, Lodi A, Ludwig C, Bunce CM, Viant MR, Günther UL. Optimized metabolite extraction from blood serum for 1H nuclear magnetic resonance spectroscopy. Anal Biochem. 2008;377:16-23.

91. Tynkkynen T. ^{1}H NMR analysis of serum lipids. Publications of the University of Eastern Finland. Dissertations in Forestry and Natural Sciences, no 76. 2012. URN:ISBN:978-952-61-0839-1

92. Wold S, Sjöström M, Eriksson L. PLS-regression: a basic tool of chemometrics. Chemometr Intel Lab. 2001;58:109-30.

93. Barker M, Rayens W. Partial least squares for discrimination. J Chemometr. 2003;17:166-73.

94. Dray S, Dufour AB. The ade4 Package: Implementing the Duality Diagram for Ecologists. J Stat Soft. 2007;22:1-20.

95. Yutin N, Galperin MY. A genomic update on clostridial phylogeny: Gram-negative spore formers and other misplaced clostridia. Environ Microbiol. 2013;15:2631-41.

Figure legends

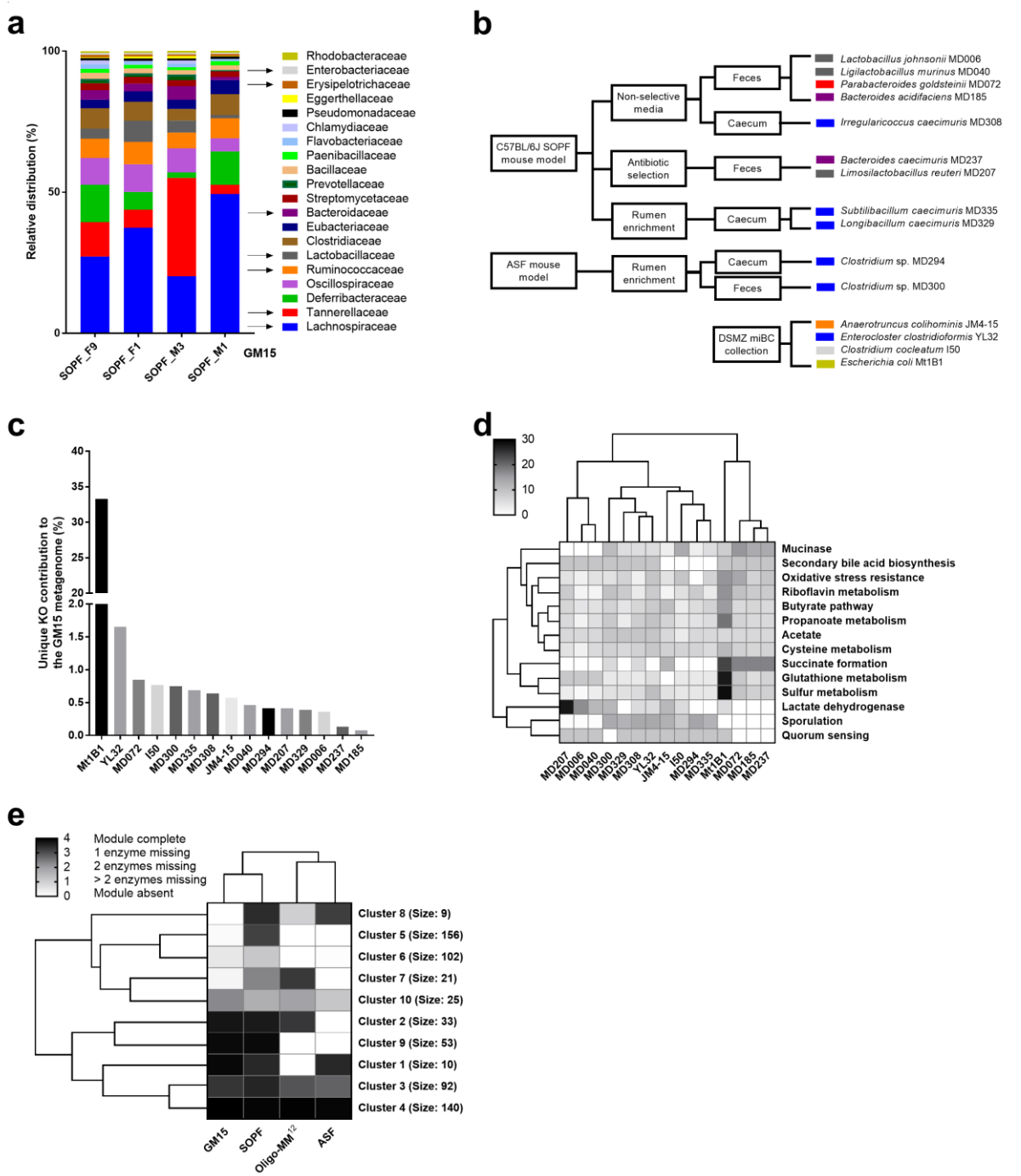

Fig. 1. Selection, isolation and functional analysis of GM15 strains. a Representative and prevalent bacterial families identified from fecal samples of 4 C57BL/6J mice of our colony. **b** 11 bacterial strains were isolated from fecal or caecal samples of either C57BL/6J or ASF mice using various culture methods. 4 additional strains were obtained from the DSMZ collection. **c** Unique KO (KEGG Orthology) groups are those present in only one GM15 member. The unique contribution of each GM15 member is relatively evenly distributed (<2%), except *E. coli*

whose unique functions contribute for 33%, although non-unique KO groups are primarily responsible for the GM15's metagenomic profile with 59% of contribution. **d** Heat map of hierarchical clustering of enzymatic activities in the gut for the 15 strains of the GM15 model. In quorum sensing (QS) function, only effector proteins were screened (because receptors suffer of similarities with nonspecific QS receptors). **e** Heat map of hierarchical clustering of KEGG modules distribution in the metagenomes of GM15, SOPF, ASF and Oligo-MM[12] models. Clusters of KEGG modules are highlighted with their respective size (number of KEGG modules). The list of KEGG modules and clusters is shown in Additional file 2: Table S1.

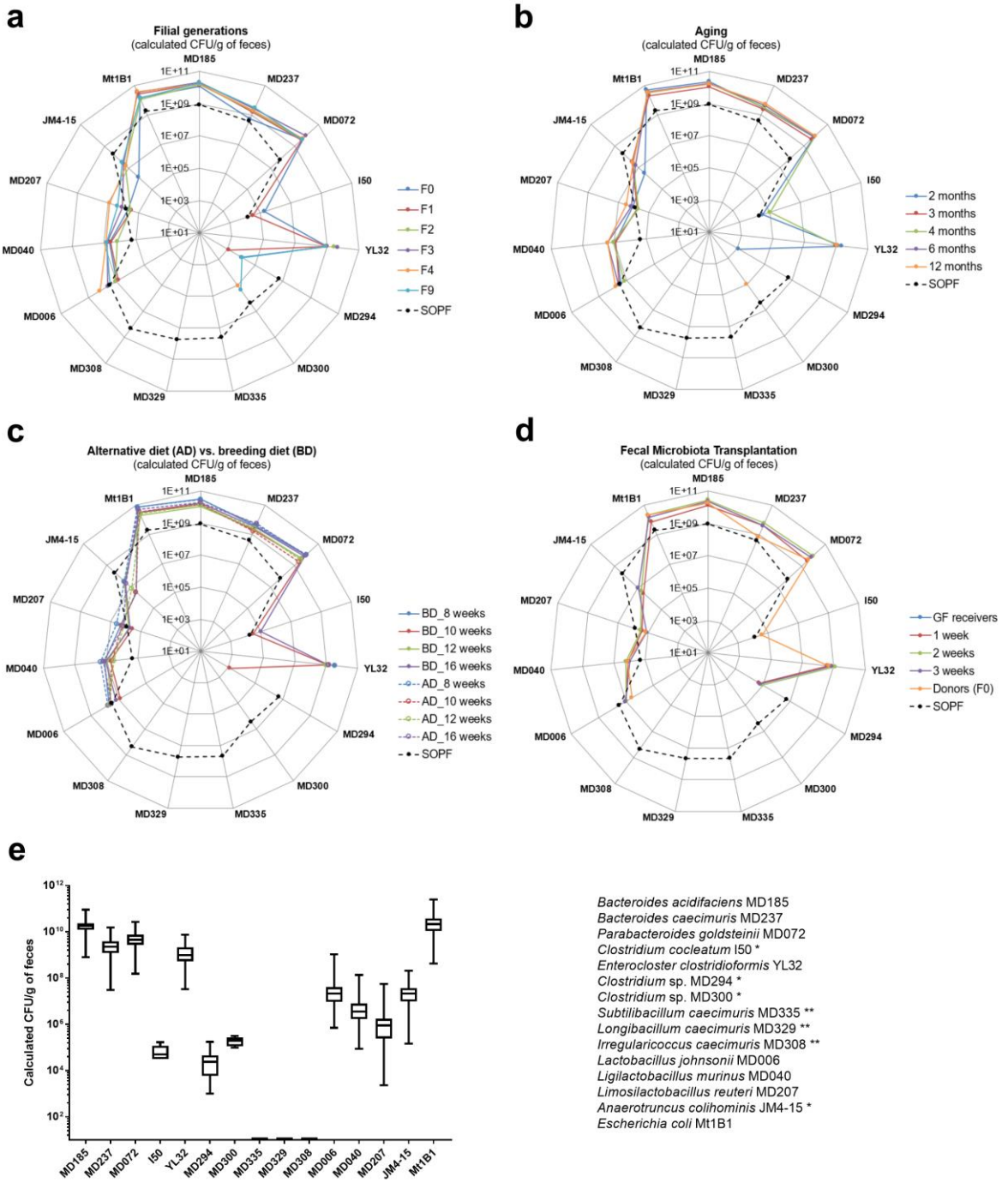

Fig. 2. Stability assessments of the GM15 mice gut microbiota over filial generations, in aging, under diet change and through FMT. a-d SOPF groups show the distribution of each GM15 strains in the complex gut microbiota of 8-week-old SOPF mice. The absolute quantification of each strain was determined by specific qPCR microfluidic assay. * Strains I50, MD294, MD300 and JM4-15 were at the detection limit of the qPCR microfluidic assay, and thus were not detected in all samples. ** Strains MD335, MD329 and MD308 were below

detection limit of the qPCR microfluidic assay. Strain YL32, obtained from the DSMZ collection, was not detected in our SOPF colony. **a** Radar plot showing the GM15 strains distribution in feces of C57BL/6J GF mice colonized with the GM15 community (F0, n=10) and bred for consecutive generations (F1 to F9, n=22 to 8). **b** Radar plot showing the overall stability of the GM15 community composition in feces collected from 9 mice between 2 and 12 months of age (2 mice died at 12-month-old). **c** Radar plot showing that an alternative diet, such as a maintenance diet, can be used for 4 weeks, and then reversed to the breeding diet for 4 more weeks, without modifying the composition of the gut microbiota of GM15 mice (n=18) compared to mice fed all along with the breeding diet (n=9). **d** Radar plot showing the feasibility of GM15 fecal microbiota transplantation to GF mice (n=9). **e** Box plots showing the low variability of the GM15 strains concentrations considering all fecal samples of mice from generation F1 to F9 (n=113), from generation F1 at 12-month-old (n=7), from generation F1 under diet change (n=18), and fecal samples collected 3 weeks post fecal microbiota transplantation in GF mice. Whiskers represent min and max data.

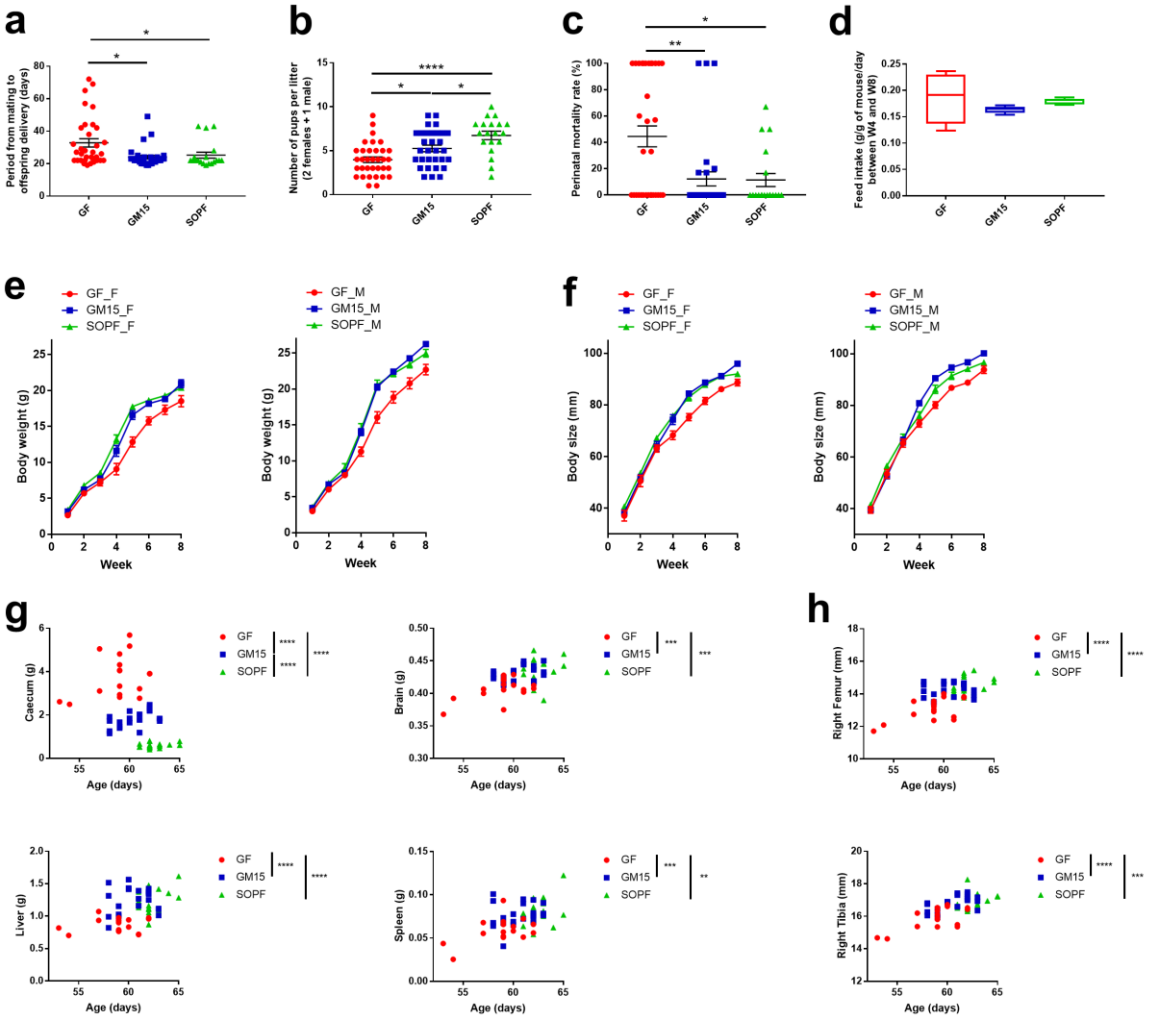

Fig. 3. Macroscopic phenotyping on mice from two consecutive filial generations (F1-F2). a-c 1-way ANOVA analyses of the reproductive performance, where dots, lines and error bars represent respectively individual litters (34 GF, 31 GM15 and 19 SOPF), means and SEM. **a** Pups delivery. Data are represented as days after mating. **b** Number of pups per litter. Data are represented as individual number. **c** Perinatal mortality. Data are represented as percentages of mortality. **d** Feed intake. Box plots and whiskers representing min and max data. **e-f** Body growth of mice bred with their mothers until week 4, where lines and error bars represent respectively means and SEM. Female (F) and male (M) respectively. Body weight and size curves. GF mice (7 F, 10 M), GM15 mice (9 F, 12 M) and SOPF mice (10 F, 10 M). **g-h** Organs weight or size impacted by age, filial generation or sex, were analyzed by the F-

test for multiple linear regressions, otherwise by 1-way ANOVA. Each animal is represented by a dot at the age of the sacrifice. *P<0.05, **P<0.01, ***P<0.001, ****P<0.0001.

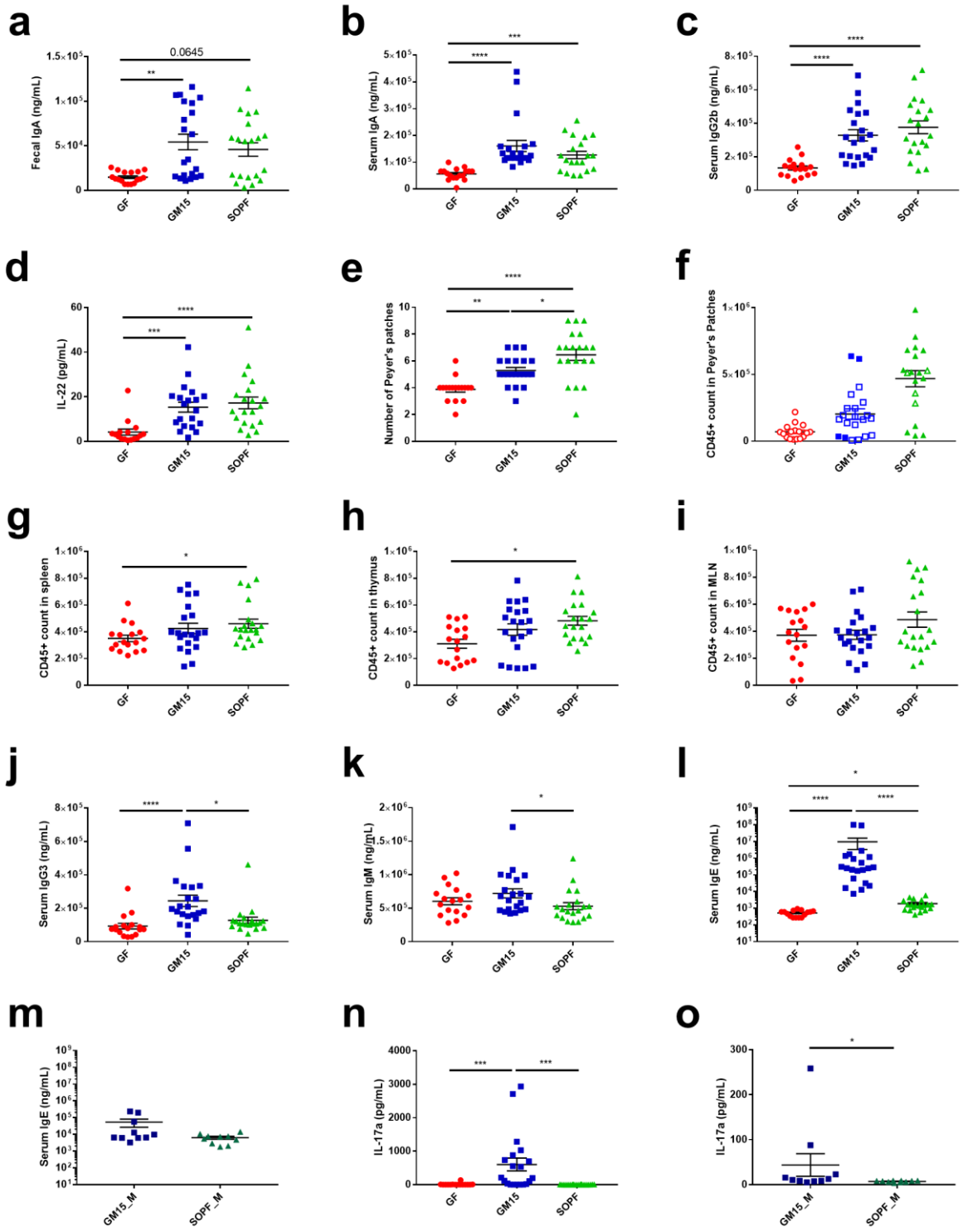

Fig. 4. Immune phenotyping through serum and fecal immunoglobulin subtyping, circulating cytokines analysis and immune cell populations analysis in different organs. **a-o** Dot plots where dots, lines and error bars represent respectively individual mice (15-17 GF, 20-21 GM15 and 20 SOPF; 10 GM15_M and 10 SOPF_M), means and SEM. **a-c** Fecal

IgA, serum IgA and IgG2b Luminex analysis. F-test for multiple linear regression analysis (fecal IgA) and Dunn's multiple comparison analyses (serum IgA, IgG2b). **d** Circulating IL-22 levels Luminex analysis. Dunn's multiple comparison analyses. **e** PP number. Tukey's multiple comparison analysis. **f** CD45+ cell count in PP. CD45+ cell count per million of viable cells stained (filled symbol) or CD45+ cell count per total viable cells stained when less than 1 M cells were isolated (empty symbol). No statistical test. **g-i** CD45+ cell count comparison in spleen, thymus and MLN by flow cytometry (CD45+ count per million of viable cells stained). Dunn's multiple comparison analyses. **j-k** IgG3 and IgM Luminex analysis. Dunn's multiple comparison analyses. **l-m** IgE Luminex analysis. Dunn's multiple comparison analyses and Mann-Whitney test respectively. **n-o** Circulating IL-17a levels Luminex analysis. Dunn's multiple comparison analyses and Mann-Whitney test respectively. *P<0.05, **P<0.01, ***P<0.001, ****P<0.0001.

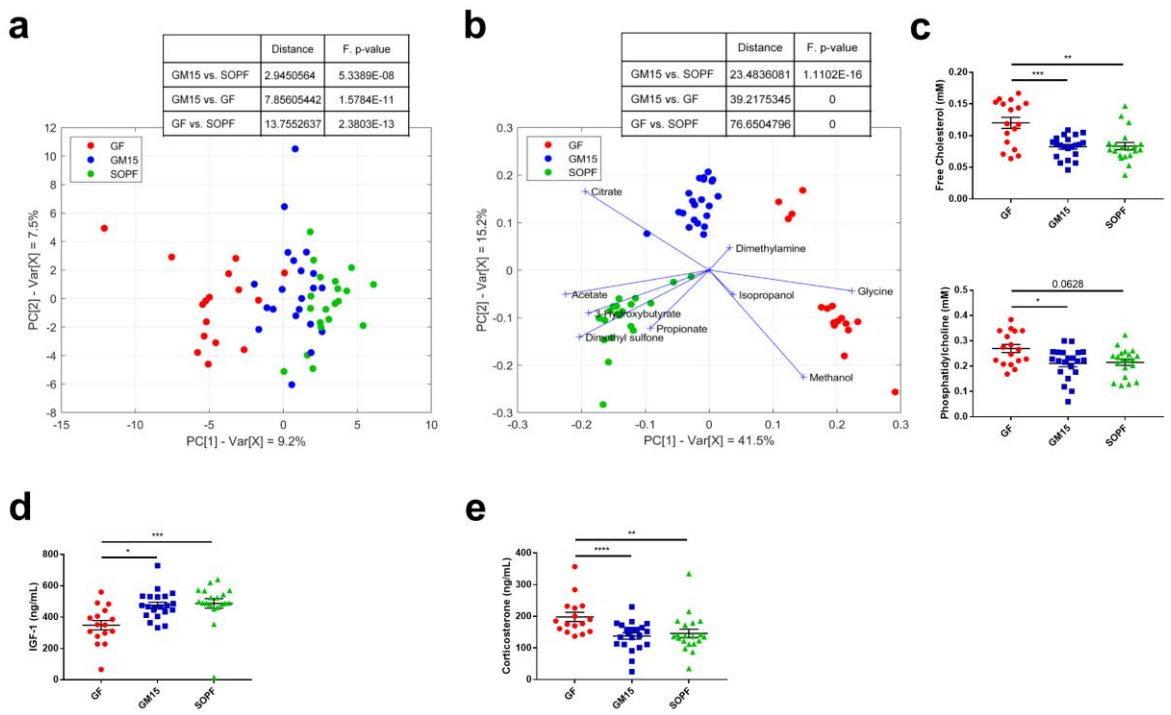

Fig. 5. Metabolic phenotyping of GM15 animals. a PCA score plot representing the distribution of the polar metabolite composition along the two first principal components. **b** Biplot representing the projection of samples in the PLS-DA score plot given by the two first components and the projection of the contribution of significant polar metabolites. **c-e** Dot plots where dots, lines and error bars represent respectively individual mice (16-17 GF, 21 GM15 and 19-20 SOPF), means and SEM. **c** F-test for multiple linear regressions representing Free Cholesterol and Phosphatidylcholine. **d** Serum IGF-1 levels Luminex analysis. Dunn's multiple comparison analysis. **e** Serum corticosterone levels Luminex analysis. F-test for multiple linear regressions.

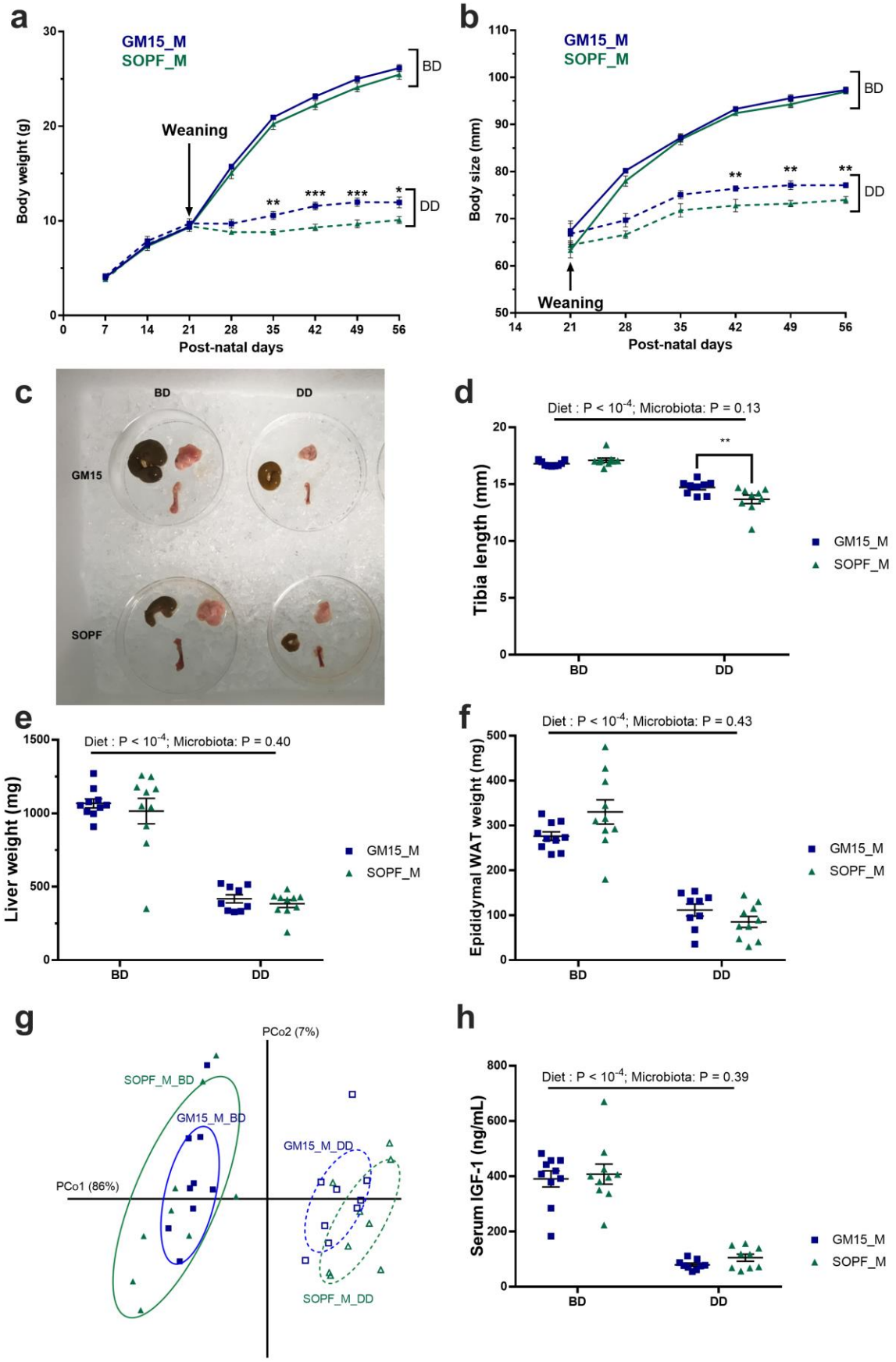
a
GM15_M
SOPF_M
Weaning
BD
DD
Body weight (g)
Post-natal days
b
GM15_M
SOPF_M
Weaning
BD
DD
Body size (mm)
Post-natal days
c
BD
DD
GM15
SOPF
d
Diet : P < 10-4; Microbiota: P = 0.13
Tibia length (mm)
GM15_M
SOPF_M
BD
DD
e
Diet : P < 10-4; Microbiota: P = 0.40
Liver weight (mg)
GM15_M
SOPF_M
BD
DD
f
Diet : P < 10-4; Microbiota: P = 0.43
Epididymal WAT weight (mg)
GM15_M
SOPF_M
BD
DD
g
PCo2 (7%)
PCo1 (86%)
SOPF_M_BD
GM15_M_BD
GM15_M_DD
SOPF_M_DD
h
Diet : P < 10-4; Microbiota: P = 0.39
Serum IGF-1 (ng/mL)
GM15_M
SOPF_M
BD
DD

1485

Fig. 6. GM15 mice and SOPF response under post-weaning chronic undernutrition. a-h Dot plots where dots, lines and error bars represent respectively individual mice (10 males per group), means and SEM. Body weight (**a**) and body size (**b**) were measured every week from weaning to post-natal day 56. **c** Representative picture of caecum, subcutaneous fat and right femur of mice at day 56. Tibia length (**d**), liver (**e**) and epididymal white adipose tissue (WAT) (**f**) weight were measured. **g** PCA of tissue weight and size under control conditions or under nutritional stress. Percentages on each axis indicate the variance associated to each coordinate. **h** Serum IGF-1 at day 56. BD: breeding diet; DD: depleted diet. P-values after two-way ANOVA were adjusted for Sidak's post-hoc test for multiple comparisons. *P<0.05, **P<0.01, ***P<0.001.

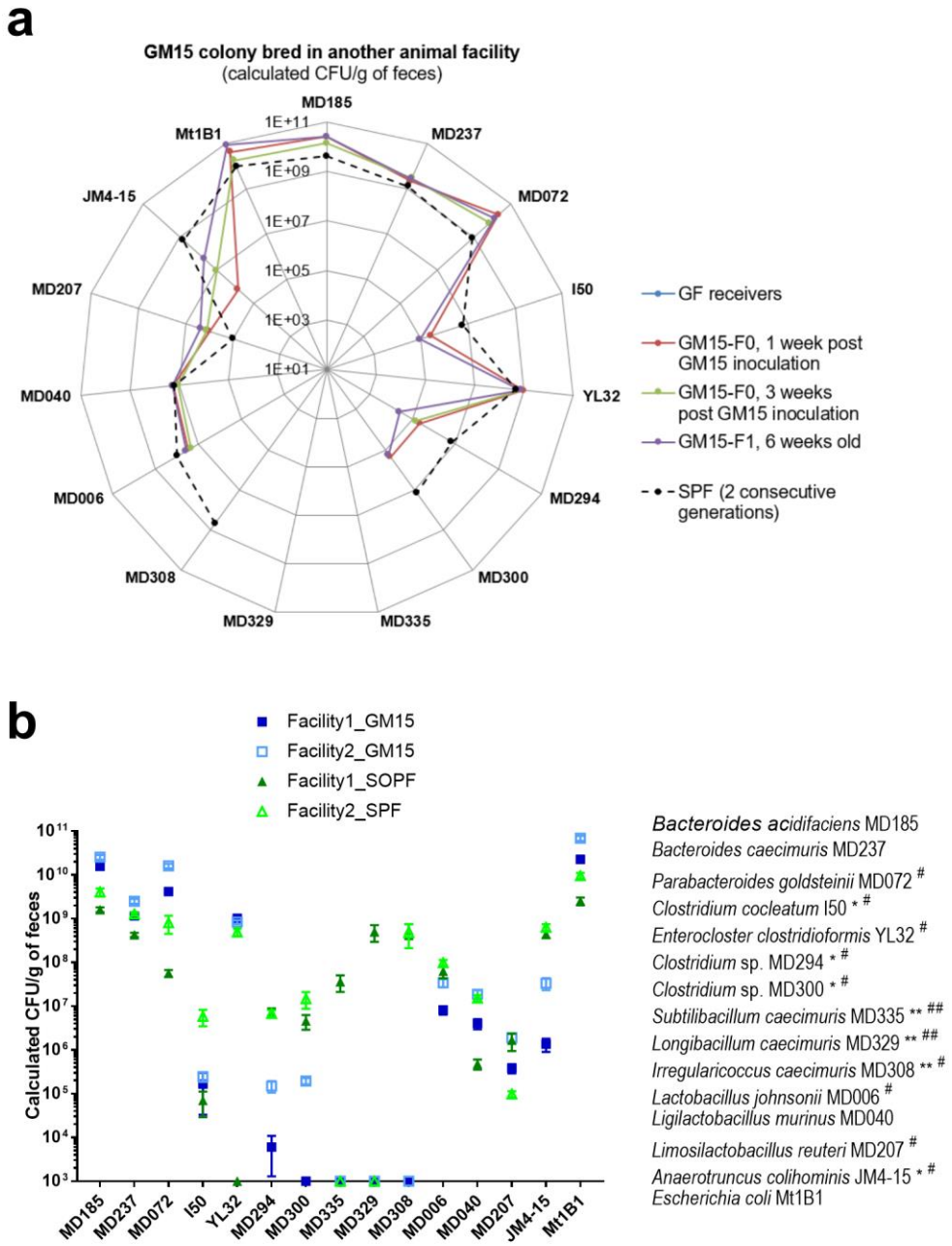

Fig. 7. The GM15 community is reproducible in another gnotobiotic facility. a-b The absolute quantification of each strain was determined by specific qPCR microfluidic assay. Strains MD072[#], I50*[#], YL32[#], MD294*[#], MD300*[#], MD308[#] MD006[#], MD207[#] and JM4-15*[#] were at the detection limit of the qPCR microfluidic assay, and thus were not detected in all GM15 (*) or SPF ([#]) samples respectively. Strains MD335**[##], MD329**[##] and MD308** were below detection limit of the qPCR microfluidic assay, and thus were not detected in any GM15 (**) or SPF ([##]) samples respectively. Strain YL32, obtained from the DSMZ collection, was not

detected in our SOPF colony (facility 1). **a** Radar plot showing the GM15 strains distribution in feces of C57BL/6J GF mice colonized in facility 2 with the GM15 community (F0, n=9) and bred for one generation (F1, n=18). SPF group shows the distribution of each GM15 strains in the complex gut microbiota of 6-8-week-old SPF mice from 2 consecutive generations. **b** Grouped plot where lines and error bars represent respectively means and SEM of GM15 strains concentrations considering fecal samples of mice (generation F0 and F1) from facility 1 (29 GM15 and 19 SOPF) and facility 2 (27 GM15 and 33 SPF).

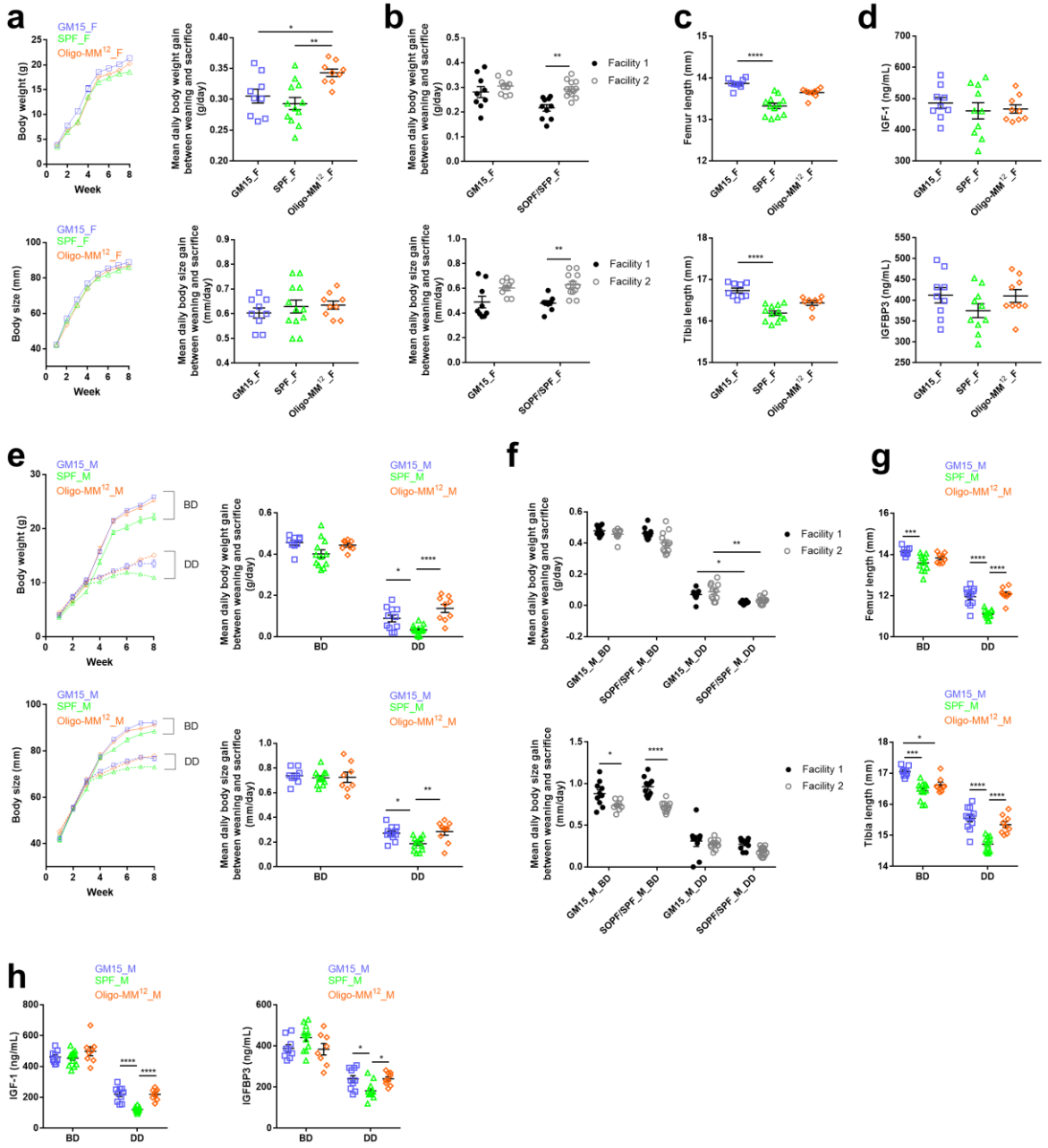

Fig. 8. The GM15 model growth and diet-induced stunting phenotypes are reproducible in another gnotobiotic facility. a-h Macroscopic phenotype of mice where dots, lines and error bars represent respectively individual mice, means and SEM. Female (F) and male (M), breeding diet (BD) and depleted diet (DD) respectively. GM15 mice (9 F, 9 M_BD, 11 M_DD), SPF mice (12 F, 12 M_BD, 13 M_DD) and Oligo-MM^{12} mice (9 F, 8 M_BD, 9 M_DD). **a** and **e** Body weight or size curves and mean daily gain of animals in facility 2. Tukey's multiple comparison analyses. **b** and **f** Mean daily body weight and size gain comparison between

GM15 and SOPF/SPF mice in facilities 1 and 2. Tukey's multiple comparison analyses. **c** and **g** 1-way ANOVA analyses of femur and tibia length. Dunn's and Tukey's multiple comparison analyses for F and M data sets respectively. **d** and **h** Serum IGF-1 and IGFB3 at day 56. Tukey's multiple comparison analyses. *P<0.05, **P<0.01, ***P<0.001, ****P<0.0001.